Computers & Fluids 105 (2014) 39–57

Contents lists available at ScienceDirect

Computers & Fluids

journal homepage: www.elsevier.com/locate/compfluid

A new robust consistent hybrid finite-volume/particle method for solving the PDF model equations of turbulent reactive flows

Reza Mokhtarpoor, Hasret Turkeri, Metin Muradoglu *

Department of Mechanical Engineering, Koc University, Rumelifeneri Yolu, Sariyer, 34450 Istanbul, Turkey

ARTICLE INFO

Article history:
Received 11 January 2014
Received in revised form 20 July 2014
Accepted 2 September 2014
Available online 10 September 2014

Keywords:
PDF methods
Consistent hybrid method
Turbulent combustion
Bluff-body flame
Swirling bluff-body flame

ABSTRACT

A new robust hybrid finite-volume (FV)/particle method is developed for solving joint probability density function (JPDF) model equations of statistically stationary turbulent reacting flows. The method is designed to remedy the deficiencies of the hybrid algorithm developed by Muradoglu et al. (1999, 2001). The density-based FV solver in the original hybrid algorithm has been found to be excessively dissipative and yet not very robust. To remedy these deficiencies, a pressure-based PISO algorithm in the open source FV package, OpenFOAM, is used to solve the Favre-averaged mean mass and momentum equations while a particle-based Monte Carlo algorithm is employed to solve the fluctuating velocity-turbulence frequency-compositions JPDF transport equation. The mean density is computed as a particle field and passed to the FV method. Thus the redundancy of the density fields in the original hybrid method is removed making the new hybrid algorithm more consistent at the numerical solution level. The new hybrid algorithm is first applied to simulate non-swirling cold and reacting bluff-body flows. The convergence of the method is demonstrated. In contrast with the original hybrid method, the new hybrid algorithm is very robust with respect to grid refinement and achieves grid convergence without any unphysical vortex shedding in the cold bluff-body flow case. In addition, the results are found to be in good agreement with the earlier PDF calculations and also with the available experimental data. Finally the new hybrid algorithm is successfully applied to simulate the more complicated Sydney swirling bluff-body flame 'SM1'. The method is also very robust for this difficult test case and the results are in good agreement with the available experimental data. In all the cases, the PISO-FV solver is found to be highly resilient to the noise in the mean density field extracted from the particles.

1. Introduction

Turbulent combustion continues to be a key technology in energy conversion systems that convert chemical energy stored in fossil fuels first into usable thermal energy and subsequently into mechanical work. Many important global issues such as energy management, climate change and pollution are directly related to the conversion of chemical energy into thermal energy via combustion that usually takes place in turbulent environment mainly due to the enhanced mixing. Accurate prediction of turbulent reacting flows is thus of fundamental importance for designing more efficient energy conversion systems and reducing the impact on the environment.

Although the Navier–Stokes equations are known to be the correct mathematical model for turbulent flows, the direct numerical simulation (DNS) is still limited to simple flows with low or moderate Reynolds numbers due to rapidly increasing computational cost with Reynolds number. In probability density function (PDF) methods, turbulent flows are modeled by a one-point, one-time joint PDF of selected flow properties. The PDF method takes full account of the stochastic nature of turbulent flows and offers the distinct advantages of being able to treat the important processes of convection and non-linear chemical reactions without any assumptions or approximations – a capability not possible by any other approaches. In particular, the exact treatment of non-linear chemical reactions makes the PDF approach highly attractive for turbulent reacting flows. Owing to these unique features, the joint PDF method coupled with a detailed chemistry model can correctly model the challenging processes of local extinction and re-ignition, i.e., the key processes that critically influence the stability of turbulent flames, quality of combustion and air pollution, as demonstrated by Xu and Pope [39] and Tang et al. [35].

As for any turbulence model, an efficient numerical solution algorithm is of crucial importance in the PDF methods. A significant progress has been made in this direction by the development

* Corresponding author. Tel.: +90 (212) 338 14 73; fax: +90 (212) 338 15 48.
E-mail address: mmuradoglu@ku.edu.tr (M. Muradoglu).

http://dx.doi.org/10.1016/j.compfluid.2014.09.006
0045-7930/

of the consistent hybrid finite-volume (FV)/particle-based Monte Carlo method [23,22,11]. It has been shown that the consistent hybrid method is up to 100 times more efficient than the best available alternative solution algorithm, i.e., the self-contained particle-mesh method implemented in *pdf2dv* code [27]. The major advantage of the hybrid method comes from the fact that it combines the best features of the FV and particle methods and avoids their respective deficiencies when used alone. It has been shown that it virtually eliminates the bias error and significantly reduces the statistical noise in mean fields [23,11]. In addition, the hybrid method can be easily coupled with existing flow solvers including the commercial CFD packages. In the original hybrid method [23,22], a density-based finite-volume solver is used to solve the mean mass, momentum and energy conservation equations while a particle-based Monte-Carlo algorithm is employed to solve the transport equation of the joint PDF for the fluctuating velocity, turbulent frequency and compositions. The method is fully consistent at the level of the governing equations since they are directly derived from the modeled joint PDF transport equation. In addition, a full consistency at the numerical level is achieved by the correction algorithms developed by Muradoglu et al. [22]. Note that the original hybrid method was implemented in loosely-coupled [23,22] and tightly-coupled [11] fashion using different finite-volume flow solvers. Here the focus is on the loosely-coupled version of the hybrid method referred as *old hybrid* algorithm from now on. Although the old hybrid method coupled with the correction algorithms has been successfully applied to various turbulent flames [3,12,14,20], it has been found to be excessively diffusive and yet not very robust mainly due to stiffness of the compressible flow equations in the incompressible or nearly incompressible limit, i.e., when Mach number $Ma \ll 1$ [12]. Preconditioning methods are commonly used to remove the stiffness of the compressible flow equations at low Mach numbers [36,37]. The major drawback of the preconditioning method is the lack of robustness especially near the stagnation points where the preconditioning matrix becomes nearly singular [7]. The preconditioning method developed by Muradoglu and Caughey [19] was incorporated into the FV solver used in the old hybrid method. In addition to the well known lack of robustness in the vicinity of stagnation points, it has been found that the preconditioning parameters are very sensitive to flow conditions and must be adjusted carefully for each flow to avoid excessive numerical dissipation while maintaining numerical stability [12]. In particular, the old hybrid algorithm failed to achieve a grid convergence for the non-reacting bluff-body flow [12]. When the grid is refined more than a threshold, the loosely-coupled hybrid solver resulted in a vortex shedding that has not been observed experimentally [5]. It was not clear whether this unphysical behavior was due to the models used or due to the excessive numerical dissipation in the density-based FV solver. The primary purpose of the present study is to remedy these deficiencies by replacing the density-based FV solver with a pressure-based FV algorithm and thus create a robust PDF solution algorithm for low Mach number flows. Here "robustness" refers to the ability of the method to maintain the stability with respect to grid refinement for a wide range of flow conditions without excessive numerical dissipation.

For this purpose, the particle based Monte Carlo algorithm is combined with the open source FV package, OpenFOAM [43], that is freely available from the Internet. The OpenFOAM package contains several pressure-based flow solvers and various turbulence models including a variety of Reynolds averaged Navier–Stokes (RANS) and large eddy simulation (LES) models. In the present study, the constant-density FV solver utilizing the PISO algorithm [10] is first modified for variable density flows and then coupled with the particle algorithm as follows: The mean velocity and mean pressure fields are supplied to the particle code by the FV solver which in turn gets all the Reynolds stresses and mean density fields from the particle code. It is emphasized here that the present hybrid algorithm is completely consistent at the level of governing equations solved by the particle and FV algorithms as in the old hybrid approach. In addition, the velocity and position correction algorithms developed by Muradoglu et al. [22] are used to enforce full consistency at the numerical solution level. The energy correction algorithm is not needed in the present hybrid method since the mean density field is obtained from the particles as a particle field and passed to the FV method. Note that the present study is the first step and paves the way for development of a general purpose RANS/PDF and LES/PDF solution algorithm for reacting turbulent flow simulations within the OpenFOAM framework. The development of LES/PDF method is underway and will be reported separately.

The new hybrid algorithm is first applied to simulate non-swirling cold and reacting bluff-body flows studied experimental by Masri et al. [16] and Dally et al. [4,5]. It is found that the new hybrid algorithm is very robust against the grid refinement demonstrating that the unphysical vortex shedding observed by Jenny et al. [12] was primarily due to excessive numerical dissipation in the density-based FV solver used in the old loosely-coupled hybrid method. The results are found to be in good agreement with the experimental data both for the non-reacting and reacting cases. It is also found that the new hybrid method predicts the flow field better than the old hybrid algorithm especially in the recirculation region. This is mainly attributed to the reduced numerical dissipation in the present FV solver and full grid convergence achieved in the present simulations. Finally the method is applied to simulate more complicated and challenging test case of the Sydney swirling bluff-body flame 'SM1'. The new hybrid algorithm is also found to be very robust for this difficult test case and the results are in good agreement with the available experimental data.

The paper is organized as follows: In Section 2, the joint velocity-turbulence frequency-compositions joint PDF model employed here are briefly reviewed. The new hybrid method and solution algorithm are described in Section 3. The results are presented and discussed in Section 4 for the cold and reacting bluff-body flows, and also for the Sydney swirling bluff-body flame. Finally conclusions are drawn in Section 5.

2. JPDF modeling

The one-point, one-time, mass-weighted JPDF of velocity $\mathbf{U}$ and compositions $\mathbf{\Phi}, \tilde{f}'$, is defined as the probability density function of the simultaneous event $\mathbf{U}(\mathbf{x},t) = \mathbf{V}$ and $\mathbf{\Phi}(\mathbf{x},t) = \mathbf{\Psi}$ where $\mathbf{V}$ and $\mathbf{\Psi}$ are the sample space variables for $\mathbf{U}$ and $\mathbf{\Phi}$, respectively. The transport equation for $\tilde{f}'$ is given by [29]

$$\frac{\partial \langle\rho\rangle \tilde{f}'}{\partial t} + V_j \frac{\partial \langle\rho\rangle \tilde{f}'}{\partial x_j} - \frac{\partial \langle p\rangle}{\partial x_j}\frac{\partial \tilde{f}'}{\partial V_j} + \frac{\partial}{\partial \psi_\alpha}\left(\langle\rho\rangle S_\alpha \tilde{f}'\right) = \frac{\partial}{\partial V_j}\left(\left\langle -\frac{\partial \tau_{ij}}{\partial x_i} + \frac{\partial p'}{\partial x_j} \middle| \mathbf{V}, \mathbf{\Psi}\right\rangle \tilde{f}'\right) + \frac{\partial}{\partial \psi_\alpha}\left(\left\langle \frac{\partial J_i^\alpha}{\partial x_i} \middle| \mathbf{V}, \mathbf{\Psi}\right\rangle \tilde{f}'\right), \quad (1)$$

where $\langle\cdot|\cdot\rangle$ stands for conditional expectation, S_α is the source term for species α due to chemical reactions, τ_{ij} is the viscous stress tensor, p' is the fluctuating component of pressure and $\mathbf{J}^\alpha$ is the diffusive fluxes. The left-hand side of the Eq. (1) is in closed form representing the evolution in time, the convection in the physical space, the transport in velocity space due to mean pressure gradient and the transport in composition space due to the chemical reactions, respectively. But the terms on the right-hand side of Eq. (1) are unclosed representing the transport in velocity space due to viscous stresses and fluctuating pressure gradient, and the transport in composition space by diffusive fluxes. The unclosed terms are modeled through construction of stochastic differential equations [29].

Table 1
Standard model constants.*

C_0	$C_{\omega 1}$	$C_{\omega 2}$	C_3	C_4	C_Ω	C_ϕ
2.1	0.5625	0.9	1.0	0.25	0.6893	2.0

* In the simulations the standard values [38] for model constants are used except for $C_{\omega 1}$ which is taken as $C_{\omega 1} = 0.65$ following Muradoglu et al. [20].

The joint velocity-turbulent frequency-compositions PDF model offers a complete closure for turbulent reacting flows [26]. The Lagrangian framework is usually preferred and the flow is represented by a large set of notional particles whose properties evolve by a set of stochastic differential equations in such a way that the particles exhibit the same JPDF as the one obtained from the solution of the modeled JPDF transport equation. The models for particle velocity, turbulent frequency, scalar mixing and reaction are discussed in this section.

Various Langevin models have been developed for the evolution of the particle velocity to account for the acceleration due to mean pressure gradient and to provide a closure for the effects of viscous dissipation and fluctuating pressure gradient [8,28]. In this study, the emphasis is placed on numerical algorithm so we employ the simplest velocity model, namely the simplified Langevin model (SLM), given by

$$dU_i^*(t) = -\frac{1}{\langle\rho\rangle}\frac{\partial\langle p\rangle}{\partial x_i}dt - \left(\frac{1}{2}+\frac{3}{4}C_0\right)\Omega\left(U_i^*(t)-\widetilde{U}_i\right)dt + \left(C_0\tilde{k}\Omega\right)^{1/2}dW_i, \tag{2}$$

where $\tilde{k}$ is the Favre mean turbulent kinetic energy and $\Omega \equiv C_\Omega \frac{\langle\rho^*\omega^*|\omega^*\geq\tilde{\omega}\rangle}{\langle\rho\rangle}$ is the conditional mean turbulent frequency with ω^* being the turbulent frequency. $\mathbf{W}(t)$ represents an isotropic vector-valued Wiener process. The standard model constants C_0 and C_Ω are introduced in [28,38], respectively, and also specified in Table 1.

Turbulent frequency ω^* is a particle property that provides the time scale needed to close the velocity and mixing models, and evolves by its own model stochastic differential equation. Here we use the modified Jayesh–Pope model [38] given by

$$d\omega^*(t) = -C_3(\omega^*-\tilde{\omega}^*)\Omega dt - S_\omega\Omega\omega^*(t)dt + (2C_3C_4\tilde{\omega}\Omega\omega^*(t))^{1/2}dW, \tag{3}$$

where the source term S_ω is defined as $S_\omega = C_{\omega 2} - C_{\omega 1}\mathcal{P}/(\tilde{k}\Omega)$. Here $\mathcal{P} = -\widetilde{u_i u_j}\frac{\partial\widetilde{U_i}}{\partial x_j}$ is the turbulence production and W is an independent Wiener process. The standard model constants are introduced in [38] and also given in Table 1.

To reduce computational cost and facilitate extensive simulations but without loss of generality, a simple flamelet model is used here for the treatment of chemical reactions. In this approach, the thermochemical state is solely determined by a single variable, the mixture fraction ξ. The flamelet library is formed based on the laminar flame calculations at a moderate stretch rate (namely $a = 100$ 1/s) using the GRI 2.1 detailed chemistry model [41]. The mixing fraction, ξ, is defined following Bilger et al. [2].

Mixing models are needed to close the molecular diffusion term, i.e., the last term in Eq. (1). There are various mixing models employed in the PDF methods [17,33]. Most scalar mixing models assume that the molecular mixing is independent of velocity, i.e., $\left\langle\frac{\partial J_i^\alpha}{\partial x_i}|\mathbf{V},\mathbf{\Psi}\right\rangle\tilde{f}' = \left\langle\frac{\partial J_i^\alpha}{\partial x_i}|\mathbf{\Psi}\right\rangle\tilde{f}'$. Although some recent works [18,31,32] indicate that this simplification can give rise to significant error, the simple interaction by exchange with the mean (IEM) mixing model is used here since the main purpose of the present study is to evaluate the performance of the new hybrid solution algorithm. Note that a more consistent mixing model has been recently proposed by Pope [24] but its performance has yet to be tested. In the IEM model [6], particle composition relaxes toward the local

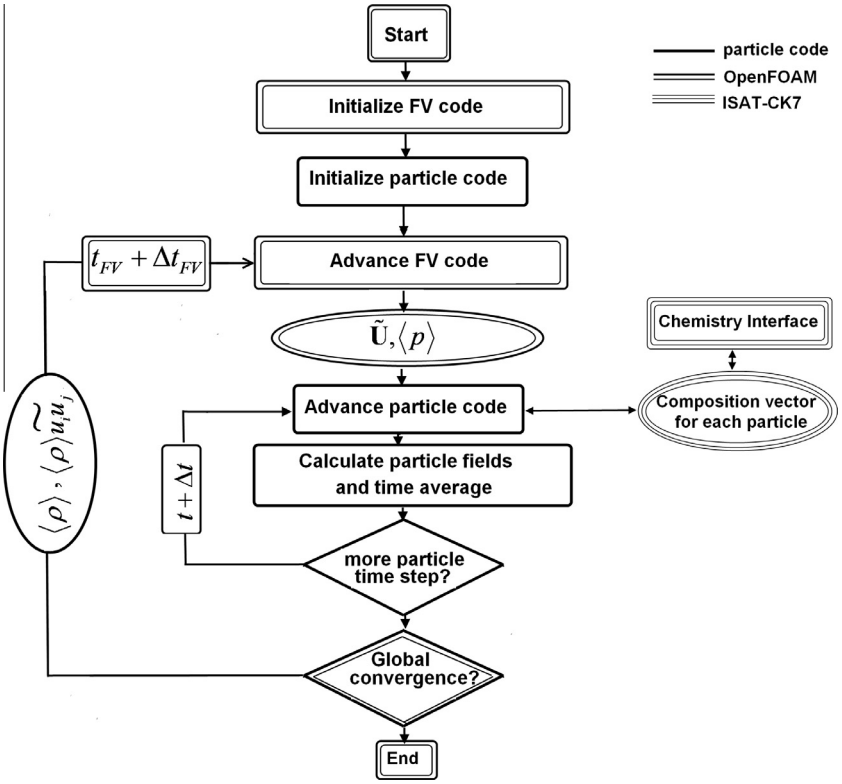

Fig. 1. Flow chart of the present hybrid method.

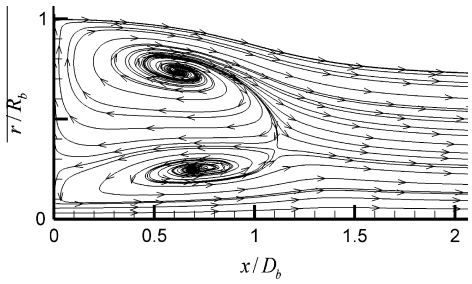

Fig. 2. The cold bluff-body flow. The mean streamlines in the vicinity of the recirculation zone computed using a 256×256 grid.

mean composition at the rate $1/2C_\phi\Omega$ and it simplifies for the flamelet model as

$$\frac{d\xi^*}{dt} = -\frac{1}{2}C_\phi\Omega(\xi^* - \tilde{\xi}^*), \tag{4}$$

where the velocity-to-scalar timescale ratio, C_ϕ, is the standard model constant specified in Table 1.

3. The new hybrid algorithm

The consistent hybrid finite-volume/particle method is the favorable solution algorithm for JPDF model equations of turbulent reactive flows. In this approach, the mean velocity and pressure are computed by the finite volume method and supplied to the particle algorithm which in turn solves the model equations for the fluctuating velocity, turbulent frequency and compositions, and provides the mean density and Reynolds stresses to the FV code. This coupling substantially reduces the noise in the mean fields used in the particle equations and thus virtually eliminates the bias error [23]. In the original consistent hybrid method proposed by Muradoglu et al. [23,22], a density-based finite-volume solver is used to solve the mean mass, momentum and energy conservation equations while a particle-based Monte-Carlo algorithm is employed to solve the stochastic equations for the fluctuating velocity, turbulent frequency and compositions. Full consistency of the method was enforced by the correction algorithms [22]. The old hybrid algorithm has been found to be excessively dissipative and yet not to be very robust mainly due to the density-based FV solvers employed to solve the mean flow equations [12]. It is well known that the compressible flow equations become stiff in the low Mach number limit and thus the density based solvers suffer from excessive numerical dissipation, lack of convergence and

Table 2
Flow parameters for the non-swirling bluff-body flame 'HM1E'.

Case	Fuel (volume ratio)	U_c (m/s)	U_j (m/s)	T_{in} (K)	ξ_{st}
'HM1E'	CH4:H2(1:1)	35	108	298	0.05

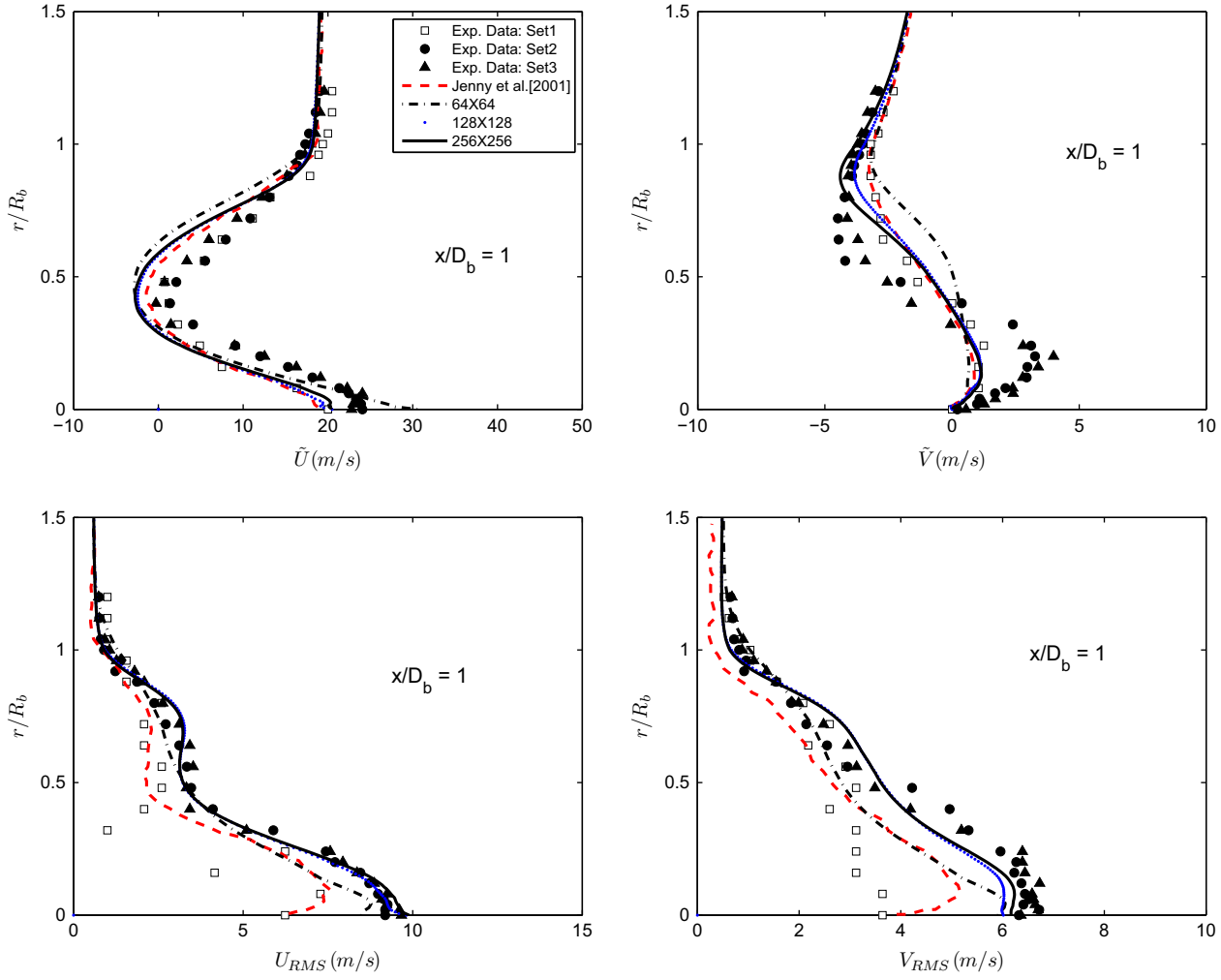

Fig. 3. The cold bluff-body flow. Radial profiles of the mean and rms axial and radial velocities at the axial location $x/D_b = 1.0$. Present results obtained using $64 \times 64, 128 \times 128$ and 256×256 grids are compared with the experimental measurements and the previous PDF results computed using the old hybrid algorithm.

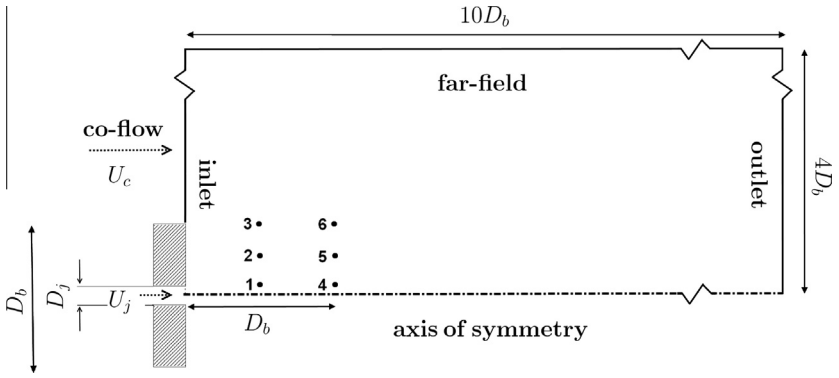

Fig. 4. Computational domain with boundary conditions for the non-swirling bluff-body flame. Locations of monitor points are shown with respect to the bluff-body base. See also Table 3.

Table 3
The coordinates of probe points used to monitor statistical stationarity.

Points	1	2	3	4	5	6
x	$D_b/2$	$D_b/2$	$D_b/2$	D_b	D_b	D_b
r	R_j	$D_b/4$	$D_b/2$	R_j	$D_b/4$	$D_b/2$

robustness [36]. Various preconditioning methods have been developed to remove the stiffness of the compressible flow equations at low Mach numbers [36,37]. The major disadvantage of the preconditioning methods is the lack of robustness especially near the stagnation points where the eigenvectors of the dissipation matrix become nearly parallel [7]. The preconditioning method developed by Muradoglu and Caughey [19] was employed in the FV solver used in the old hybrid method. In addition to the well known lack of robustness in the vicinity of stagnation points, it has been found that the solution is highly sensitive to the preconditioning parameters and may be contaminated by the excessive numerical dissipation unless the preconditioning parameters are carefully tuned for each flow [12]. In particular, the old hybrid algorithm failed to achieve a grid convergence for the non-reacting bluff-body flow [12]. When the grid is refined beyond a threshold, the loosely-coupled hybrid solver [22] resulted in a vortex shedding that has not been observed experimentally [5].

The present hybrid method is designed to remedy the deficiencies of the old hybrid algorithm and thus create a robust PDF solution algorithm for a wide range of flow conditions without any adjustable free parameter. In this approach, a pressure-based FV solver is employed to solve the Favre-averaged variable density incompressible flow equations while a particle-based Monte Carlo algorithm is used to solve the evolution equations for the fluctuating velocity, turbulent frequency and compositions. For this purpose, the constant-density PISO-FV solver that is available in

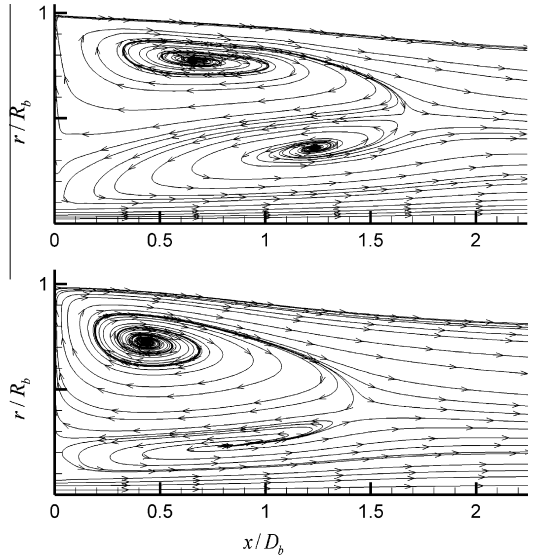

Fig. 6. The non-swirling bluff-body HM1E flame. The mean streamlines in the recirculation zone computed using the new algorithm (top plot) and the old hybrid algorithm (bottom plot).

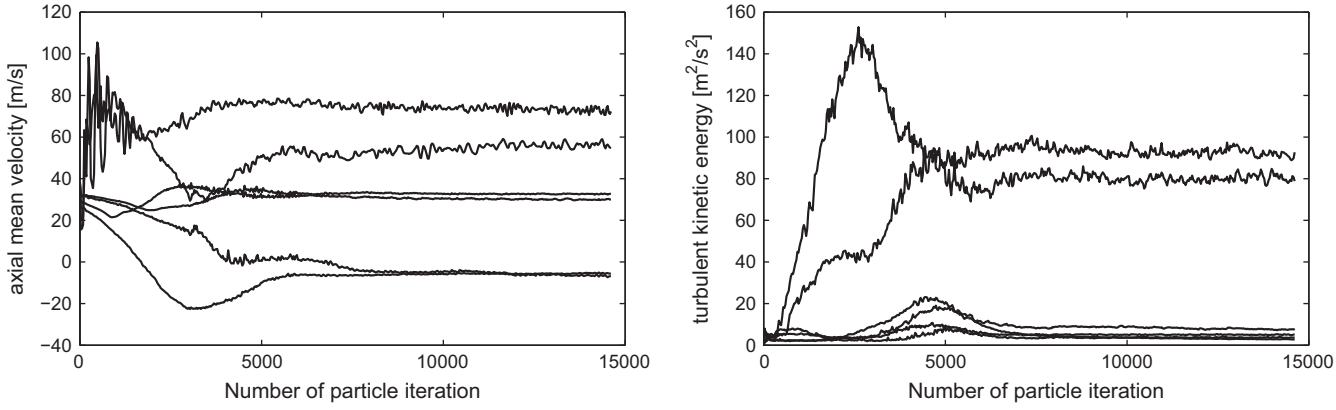

Fig. 5. The non-swirling bluff-body HM1E flame. Time series of Favre-averaged mean axial velocity and turbulent kinetic energy at the six probe points.

OpenFOAM package [43] has been first modified for a variable density flow and then combined with the particle code. The mean density field is obtained from the particles as a particle field and passed to the FV solver. Note that this is in contrast with the old hybrid method in which the mean energy equation is solved by the FV solver and the mean density is subsequently obtained from the mean equation of state. As a result, the redundant FV density field and associated energy correction used in the old hybrid method are eliminated in the present approach. In the next sections the equations solved by the FV and particle algorithms are first described and then the coupling is discussed.

3.1. FV system

The open source FV package OpenFOAM is employed to solve the mean mass and momentum equations using a pressure based PISO algorithm. The conservation equations are directly derived from the modeled JPDF evolution equation and can be written as

$$\frac{\partial\langle\rho\rangle}{\partial t}+\frac{\partial}{\partial x_i}(\langle\rho\rangle\widetilde{U}_i)=0, \tag{5}$$

$$\frac{\partial}{\partial t}\left(\langle\rho\rangle\widetilde{U_i}\right)+\frac{\partial}{\partial x_j}\left(\langle\rho\rangle\widetilde{U_i}\widetilde{U_j}\right)=-\frac{\partial\langle p\rangle}{\partial x_i}-\frac{\partial}{\partial x_j}(\langle\rho\rangle\widetilde{u_iu_j}). \tag{6}$$

Assuming that the flow is statistically stationary, the time derivative in the mass conservation equation can be neglected and the continuity equation becomes

$$\frac{\partial}{\partial x_i}(\langle\rho\rangle\widetilde{U}_i)=0. \tag{7}$$

The mean mass and momentum equations are closed since the mean density $\langle\rho\rangle$ and the Reynolds stresses $\langle\rho\rangle\widetilde{u_iu_j}$ are evaluated as particle mean fields and passed to the FV code in each outer iteration. These particle quantities are time-averaged using the same procedure as Muradoglu et al. [22] to reduce the statistical error. Note that the FV solver is found to be very robust even if the mean density and Reynolds stresses are not time-averaged and contain significant statistical fluctuations. This is of crucial importance especially for unsteady RANS/PDF or LES/PDF simulations.

3.2. Particle system

In the context of the hybrid method, the particle algorithm is used to solve the evolution equations for the fluctuating velocity, turbulence frequency and compositions. The mean velocity field is taken from the FV solver. Therefore, the mean velocity evolution equation is subtracted from the velocity model to obtain the

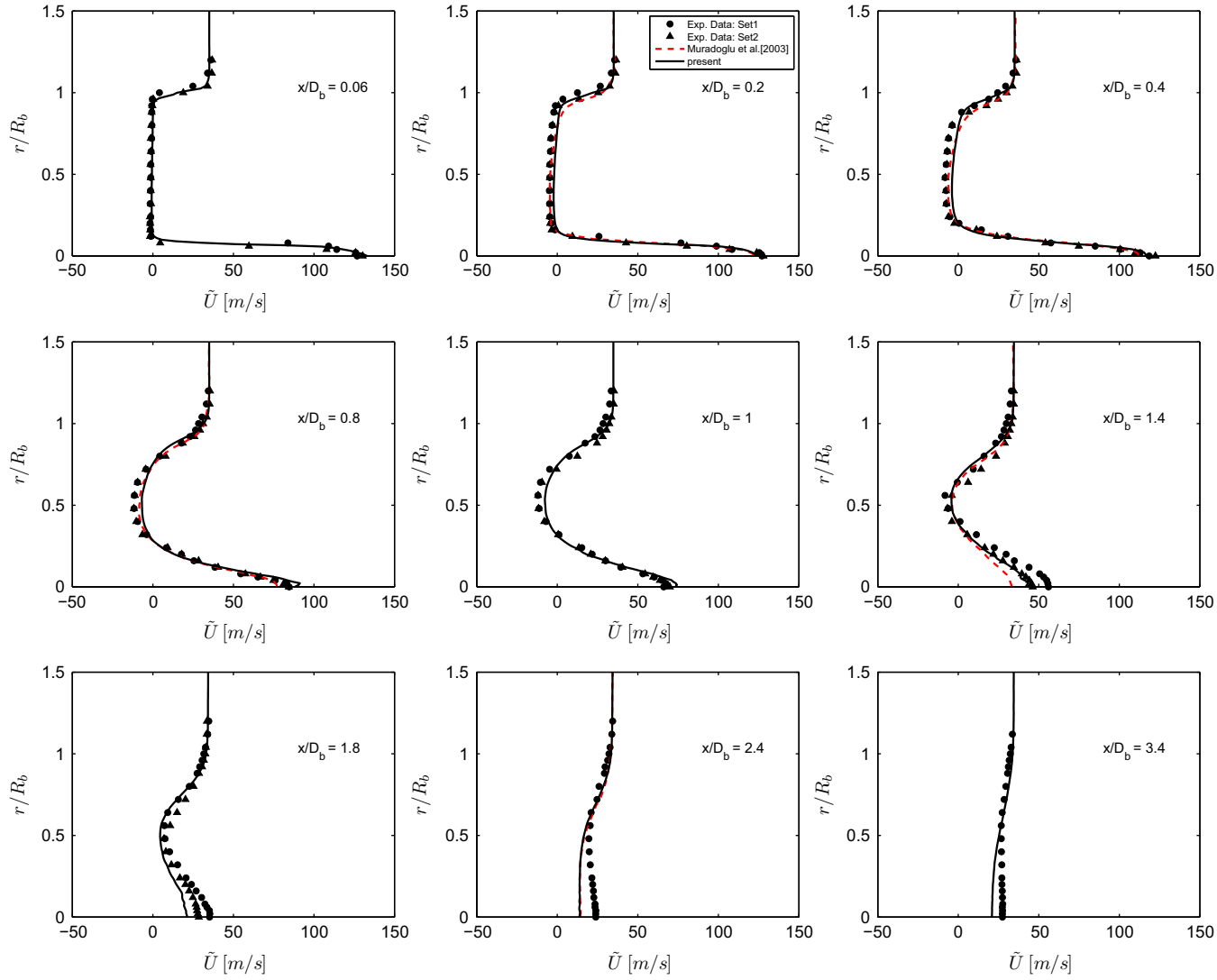

Fig. 7. The non-swirling bluff-body HM1E flame. Radial profiles of mean axial velocity compared with the experimental data (symbols) and the earlier PDF simulation of Muradoglu et al. [20] (red dashed lines). (For interpretation of the references to colour in this figure legend, the reader is referred to the web version of this article.)

evolution equation for the fluctuating part. The SLM model for the fluctuating part of the velocity is then given by

$$du_i^* = \frac{1}{\langle\rho\rangle}\frac{\partial(\langle\rho\rangle\widetilde{u_i u_j})}{\partial x_j}dt - u_j^*\frac{\partial \widetilde{U}_i^*}{\partial x_j}dt - \left(\frac{1}{2}+\frac{3}{4}C_0\right)\Omega u_i^*(t)dt + \left(C_0\tilde{k}\Omega\right)^{1/2}d\mathcal{W}_i. \quad (8)$$

The particles move with the local flow velocity according to

$$d\mathbf{X}^* = \left(\tilde{\mathbf{U}}^* + \mathbf{u}^*\right)dt, \quad (9)$$

where $\tilde{\mathbf{U}}^*$ is the Favre-averaged mean velocity interpolated from the FV field on the particle locations while $\mathbf{u}^*$ is obtained from solution of Eq. (8). Note that the interpolation scheme developed by Jenny et al. [11] is used to evaluate $\tilde{\mathbf{U}}^*$ in Eq. (9). The particle algorithm also solves the evolution equations for the turbulent frequency (Eq. (3)) and compositions (Eq. (4)).

3.3. Coupling

The FV and particle methods are periodically used in the hybrid algorithm to solve their respective equations as shown in Fig. 1. Following Muradoglu et al. [23,22], each period is called an outer iteration which consists of FV and particle inner iterations. The mean density and Reynolds stresses are obtained from the particle code and kept the same during each FV inner iteration. Then mean velocity and pressure are passed to the particle code that is run for a few (typically 3) time steps in each particle inner iteration.

The particle fields needed to close the equations solved by the FV and particle algorithms are computed using the cloud-in-cell (CIC) method [9] and subsequently time-averaged to reduce the statistical error. Following Muradoglu et al. [22], a particle mean field Q is time-averaged as

$$Q_{TA}^k = \left(1-\frac{1}{N_{TA}}\right)Q_{TA}^{k-1} + \frac{1}{N_{TA}}Q^k, \quad (10)$$

where Q_{TA}^k and Q^k are the time-averaged and instantaneous values evaluated at kth particle time step. The parameter N_{TA} is a time-averaging factor that is selected relatively small in the initial stage of simulation and gradually increased to its final value when a statistically stationary solution is reached. The FV fields are not time-averaged.

Although the present hybrid method is fully consistent at the level of governing equations, inconsistencies may occur due to accumulation of numerical error. Velocity and position correction algorithms developed by Muradoglu et al. [22] are employed to

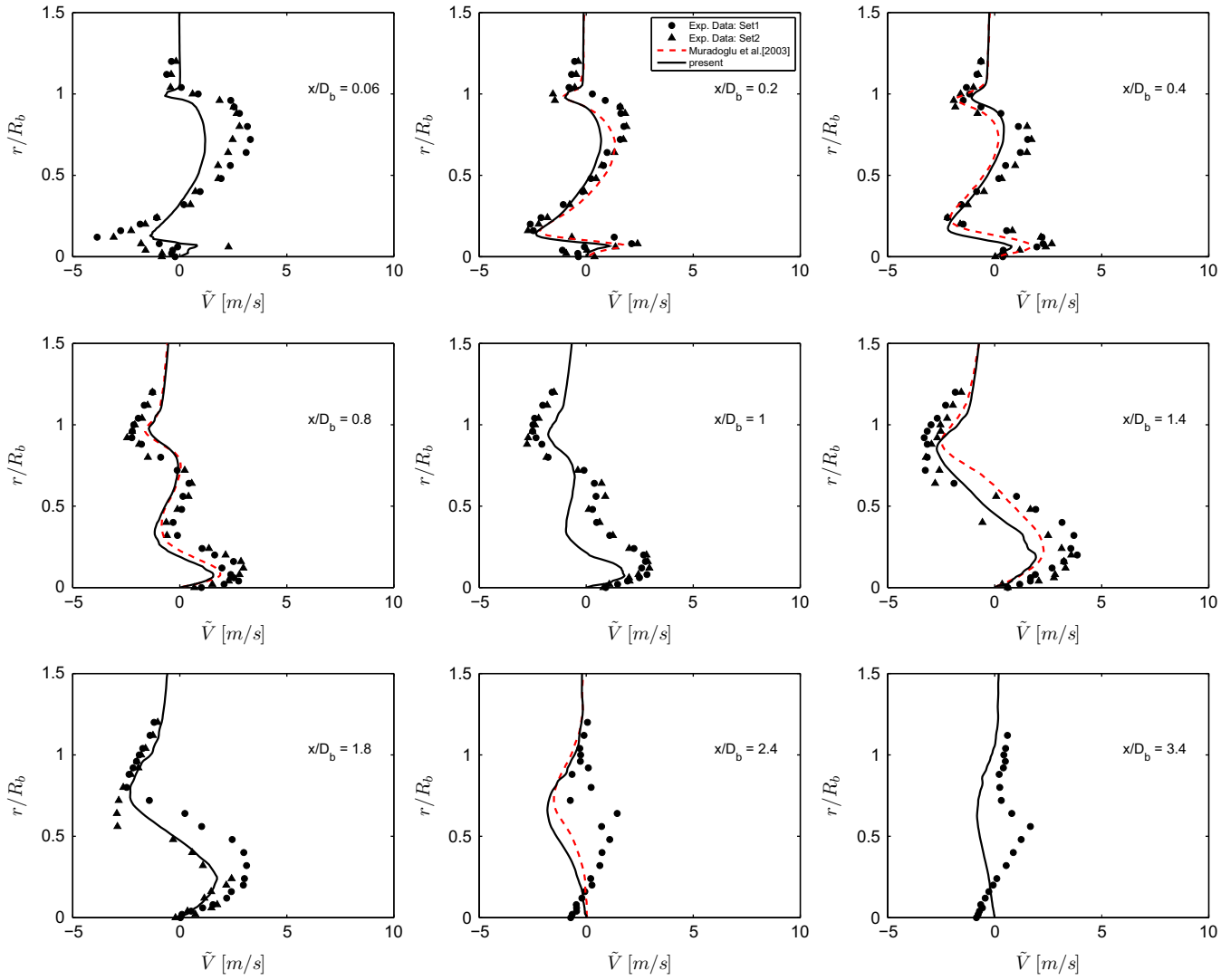

Fig. 8. The non-swirling bluff-body HM1E flame. Radial profiles of mean radial velocity compared with the experimental data (symbols) and the earlier PDF simulation of Muradoglu et al. [20] (red dashed lines). (For interpretation of the references to colour in this figure legend, the reader is referred to the web version of this article.)

achieve a full consistency at the numerical solution level. Local time stepping is an effective way of accelerating convergence to a statistically stationary state when a highly stretched non-uniform grid is used. In the present study, the local time stepping method developed by Muradoglu and Pope [21] is also employed to accelerate the convergence rate significantly.

Although the chemistry model employed in this study is relatively simple and requires only interpolation of the thermochemical quantities from the flamelet table as a function of mixture fraction, ISAT [25] algorithm is incorporated into the hybrid method to allow simulations with detailed chemistry. Note that application of the new hybrid method to premixed stratified flames [34] with a detailed chemistry model is underway and will be reported separately.

4. Results and discussions

The new hybrid algorithm is first applied to non-swirling cold and reacting bluff-body flows studied experimentally by Masri et al. [16] and Dally et al. [4,5]. Computations are first performed for the cold bluff-body flow to demonstrate the robustness of the present hybrid method with respect to grid convergence and resolve the uncertainty about the unphysical vortex shedding observed in the previous PDF simulations using the old hybrid method [12]. Extensive simulations are then performed for the reacting bluff-body flame 'HM1E' to assess the numerical properties and performance of the present hybrid approach. Subsequently the method is applied to more challenging case of swirling bluff-body stabilized turbulent flame studied experimentally by the Syndey group [1,13,15]. The main purpose of the swirling flame test case is to demonstrate the robustness of the present hybrid method for this challenging flow. Thus only a few representative results are included in the present paper. A full description of the PDF simulations of the swirling bluff-body flames using both a simple flamelet and a detailed chemistry (e.g., ARM2) models will be reported separately.

4.1. Sydney bluff-body burner

The bluff-body flames have been selected among the target flames in the turbulent non-premixed flames (TNF) workshops [42] due to their relevance to numerous engineering applications such as bluff-body stabilized combustors widely used in industrial applications because of their enhanced mixing characteristics, improved flame stability and ease of combustion control [4,5]. Besides their practical significance, the bluff-body flows provide

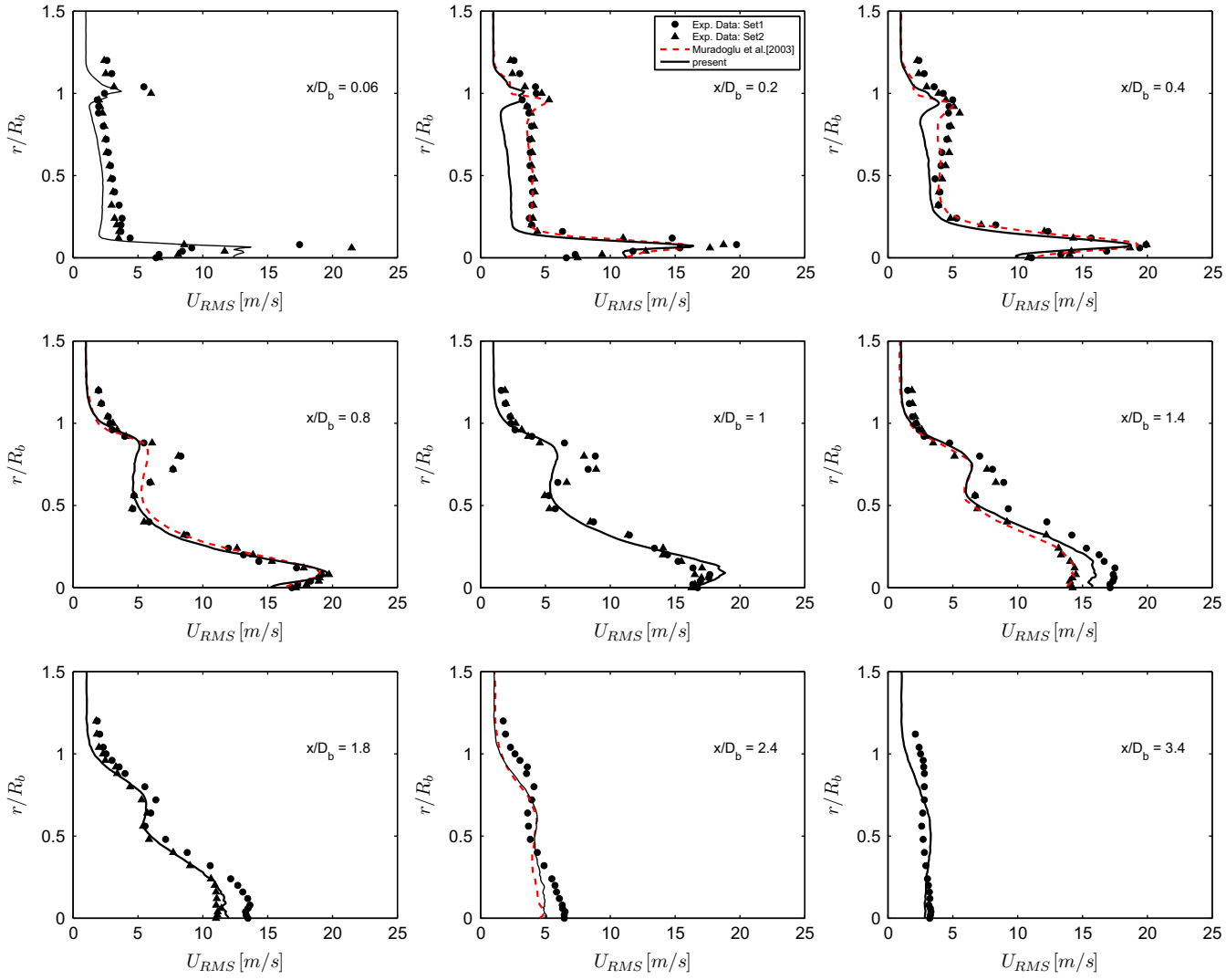

Fig. 9. The non-swirling bluff-body HM1E flame. Radial profiles of rms axial velocity compared with the experimental data (symbols) and the earlier PDF simulation of Muradoglu et al. [20] (red dashed lines). (For interpretation of the references to colour in this figure legend, the reader is referred to the web version of this article.)

an excellent but challenging test case for the numerical solution algorithms as well as the chemistry and turbulence models due to their simple and well defined initial and boundary conditions, and their ability to maintain the flame stabilization for a wide range of inlet flow conditions with a complex recirculation zone [4,16]. For the bluff body flame, extensive measurements of temperature, compositions, and emission of pollutants have been made for a range of flame conditions with various fuel mixtures. The data are collected at different axial and radial locations along the full length of the most flames and are presented in the form of ensemble means, root-mean-square (rms) fluctuations, probability density functions (PDF) and scatter plots. All the experimental data are available from the Internet [42,44].

A full description of the Sydney bluff-body burner and the measurement locations can be found in [4,16,44]. In this burner a fuel jet is surrounded by a bluff body and a co-flowing air stream. The burner is placed in a wind tunnel that has an exit cross section of $230 \times 230\ \text{mm}^2$. The diameter of the bluff body is $D_b = 50$ mm, and that of the jet is $D_j = 2R_j = 3.6$ mm. There is a recirculation zone immediately after the bluff-body surface which stabilizes the flame. Downstream of the recirculation zone is called the neck zone where strong turbulence–chemistry interactions take place. Thus a simple flamelet model is expected to be less accurate in this region. Experiments were performed for various fuels and flow conditions. In the next sections we will present some simulation results of the cold bluff-body flow and then numerical properties and performance of our new algorithm are demonstrated for the bluff-body stabilised 'HM1E' flame.

4.2. Cold bluff-body flow

The cold bluff-body flow has been studied experimentally by Dally et al. [5]. The experimental data are available from the Internet [44]. There are three sets of data for this flow. The first data set (*set*1) was taken in 1995 while the other sets (*set*2 and *set*3) were measured in 1998 by the same group using more advanced experimental techniques. Thus the *set*2 and *set*3 are expected to be more accurate. Both the jet and co-flow consist of constant density air with mean velocities of 61 m/s and 20 m/s, respectively. PDF simulations of this flow were carried out using the old hybrid algorithm by Jenny et al. [12]. They found that the old loosely-coupled hybrid algorithm resulted in unphysical vortex shedding when the grid was refined beyond a threshold, i.e., the grid containing 64×64 cells. It was not clear whether this unphysical behavior was due to the deficiency of models used or due to excessive numerical dissipation in the numerical solutions. Therefore the new hybrid method is used to simulate this flow using the same sub-models, initial and boundary conditions as in Jenny et al. [12].

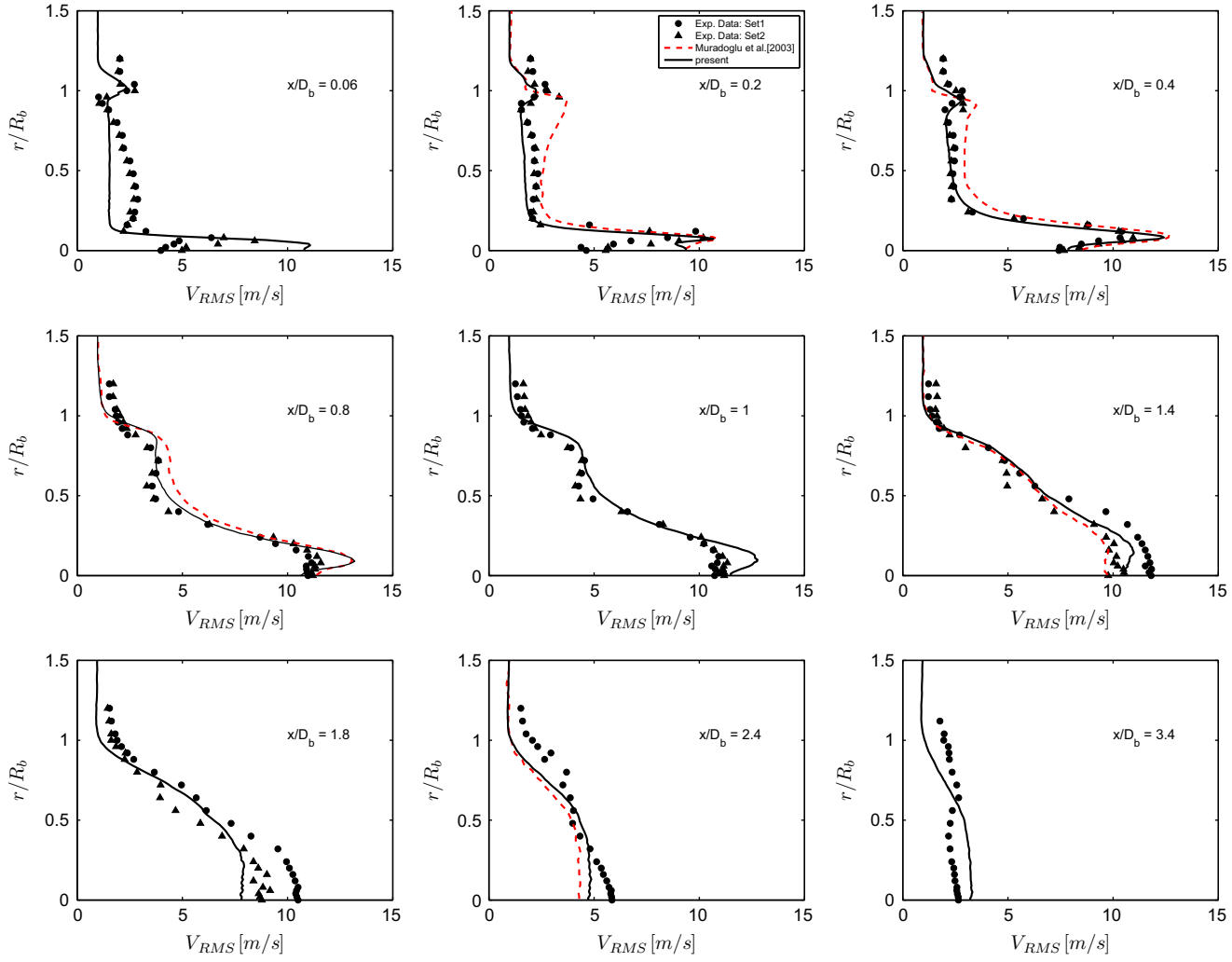

Fig. 10. The non-swirling bluff-body HM1E flame. Radial profiles of rms radial velocity compared with the experimental data (symbols) and the earlier PDF simulation of Muradoglu et al. [20] (red dashed lines). (For interpretation of the references to colour in this figure legend, the reader is referred to the web version of this article.)

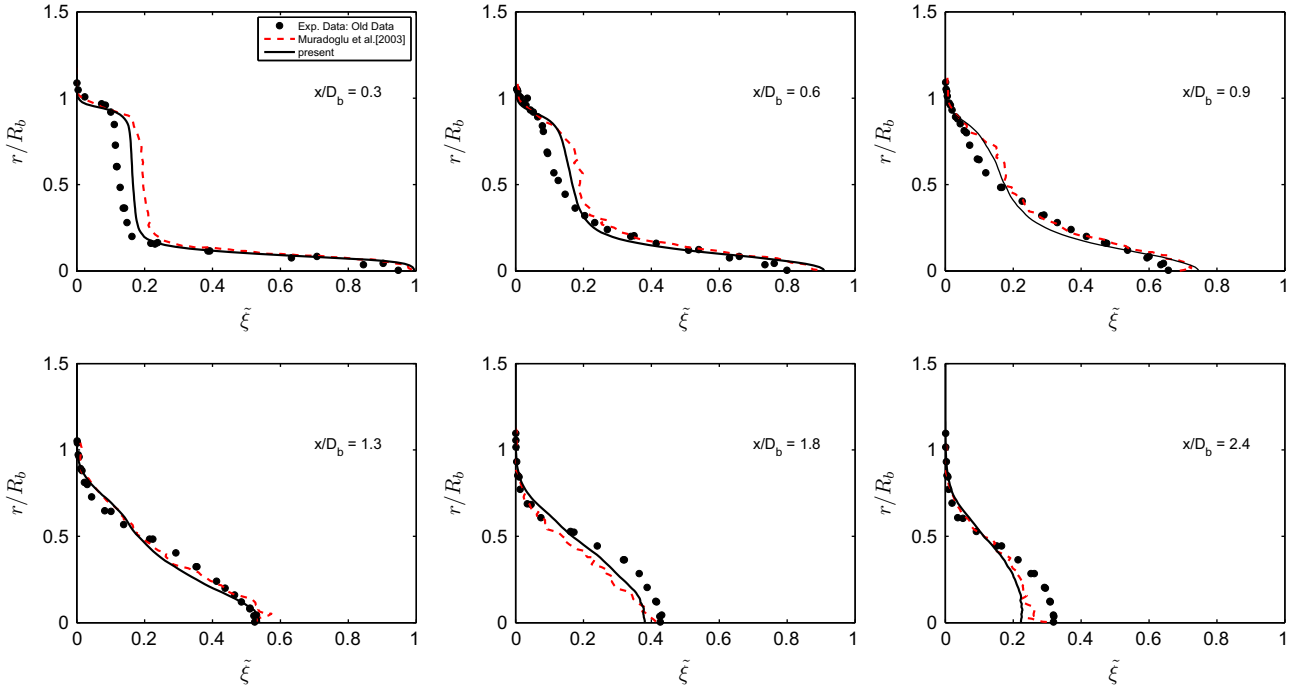

Fig. 11. The non-swirling bluff-body HM1E flame. Radial profiles of mean mixture fraction compared with the experimental data (symbols) and the earlier PDF simulation of Muradoglu et al. [20] (red dashed lines). (For interpretation of the references to colour in this figure legend, the reader is referred to the web version of this article.)

Computations are performed using $64 \times 64, 128 \times 128$ and 256×256 grids. Fig. 2 shows the mean streamlines in the vicinity of the recirculation zone (RZ) computed using the 256×256 grid. Although not shown here due to space consideration, the present hybrid algorithm reaches a statistically stationary solution successfully after about 10000 time steps without any sign of vortex shedding even for the 256×256 grid. This demonstrates that the unphysical vortex shedding observed by [12] was mainly caused by the excessive numerical dissipation in the density-based FV solver used in the old hybrid method. The flow field depicted in Fig. 2 is qualitatively in good agreement with the experimental observations [5]: There are two vortices, i.e., an outer vortex located close to the co-flowing air with the center at about $(x/D_b, r/R_b) \approx (0.7, 0.25)$ and an inner vortex located between the outer vortex and the central jet with the center at $(x/D_b, r/R_b) \approx (0.6, 0.75)$. The length of the recirculation region is predicted as $\ell_r/D_b \approx 1.1$ which compares reasonably well with the experimental value of $\ell_r/D_b \approx 1$ [5]. The radial profiles of the

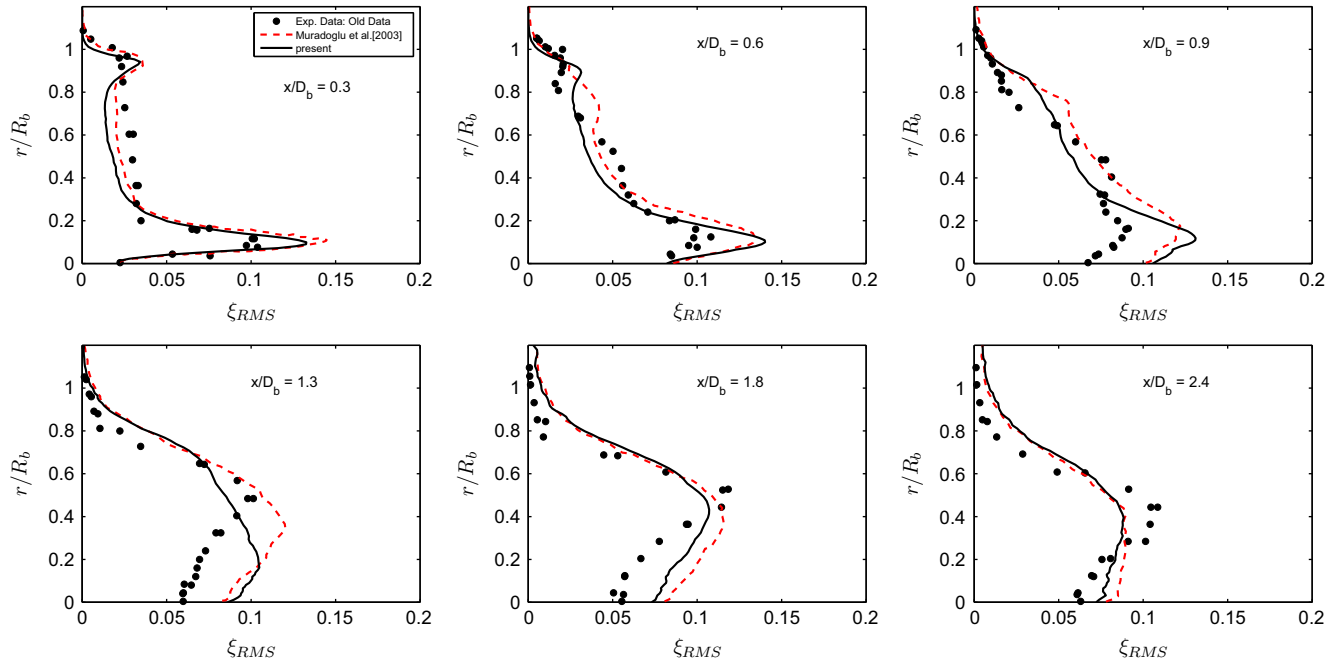

Fig. 12. The non-swirling bluff-body HM1E flame. Radial profiles of rms mixture fraction compared with the experimental data (symbols) and the earlier PDF simulation of Muradoglu et al. [20] (red dashed lines). (For interpretation of the references to colour in this figure legend, the reader is referred to the web version of this article.)

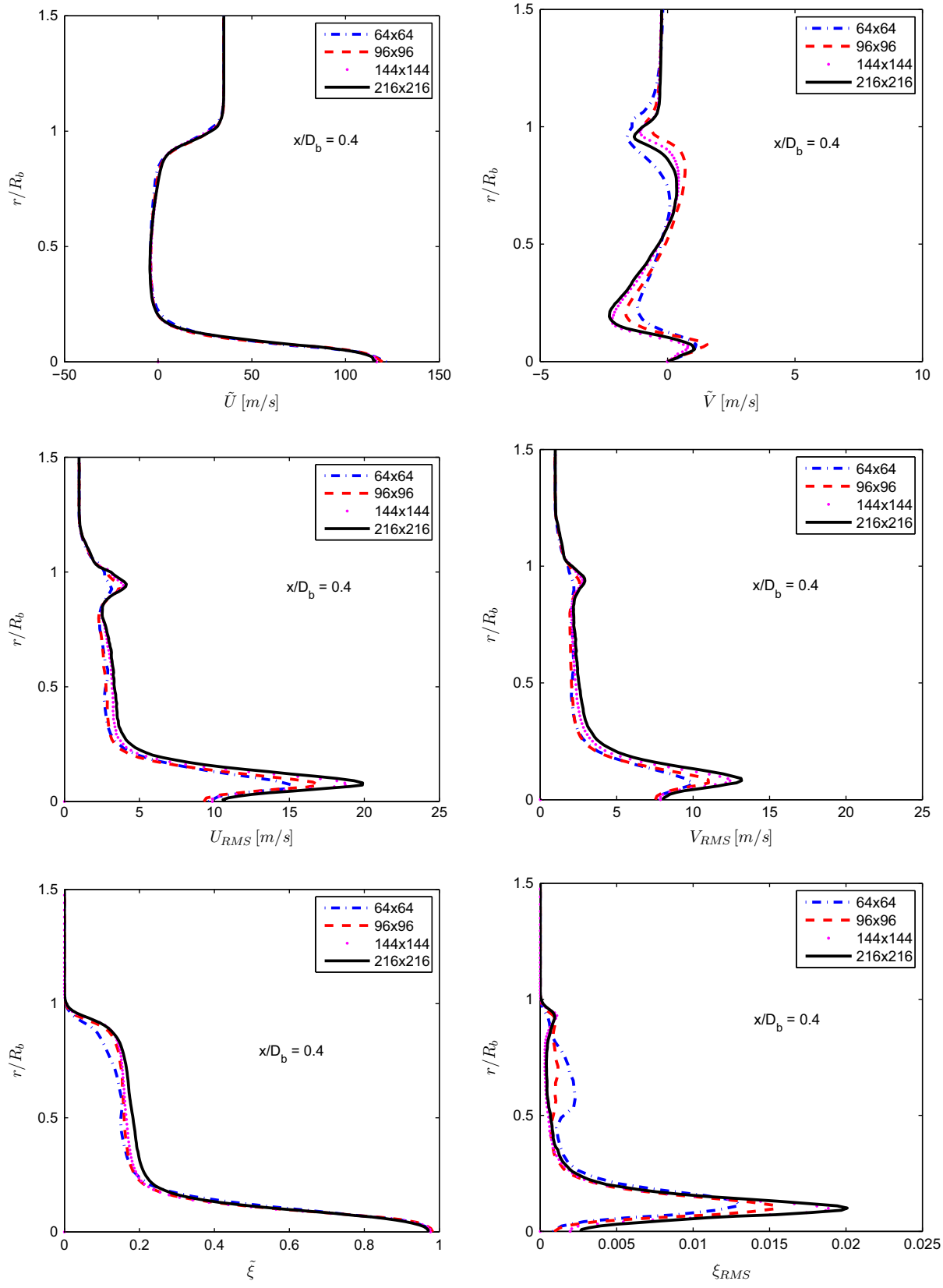

Fig. 13. Grid convergence for the non-swirling bluff-body HM1E flame: radial profiles of mean and rms fluctuating axial and radial velocities, mean and rms mixture fraction at axial location $x/D_b = 0.4$.

mean and rms velocities in the axial and radial directions computed using three different grids are plotted in Fig. 3 at axial location $x/D_b = 1.0$ and compared with the experimental data as well as with the PDF simulations performed using the old loosely coupled hybrid method [12]. As seen in this figure, the grid convergence is achieved for the 128×128 grid. In addition, the present results

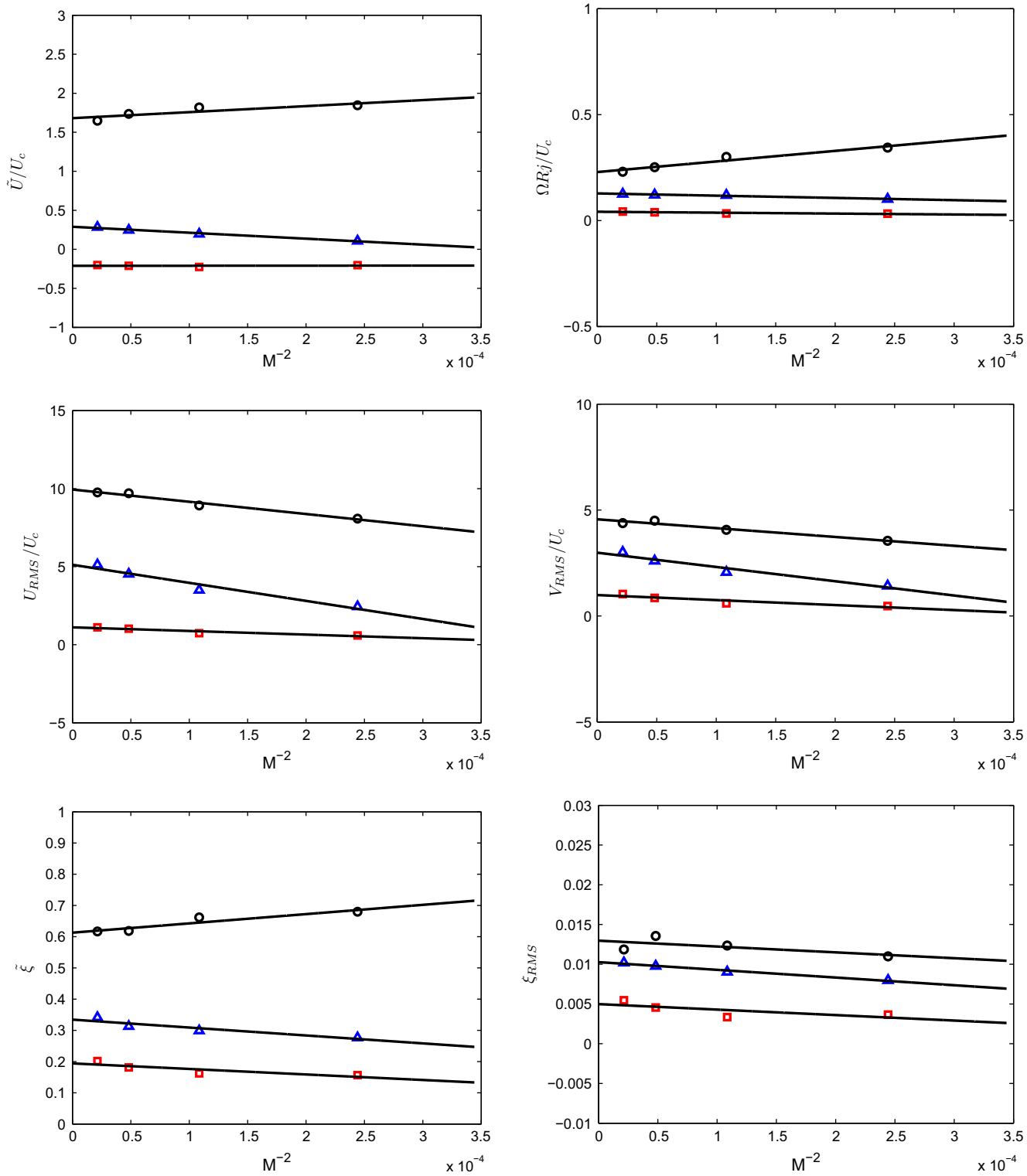

Fig. 14. Grid convergence for the non-swirling bluff-body HM1E flame: mean and fluctuating quantities against M^{-2} at selected points. Circles indicate the location at $(x/D_b = 1.0, r/R_j = 1)$, triangles at $(x/D_b = 1.0, r/R_b = 0.5)$, squares at $(x/D_b = 1.0, r/R_b = 1.0)$, and the solid lines show the linear least squares fits to the computational results.

are in better agreement with the experimental data than the results of Jenny et al. [12]. The profiles at other axial locations are not shown here due to space consideration but we state that the present results are overall in better agreement with the experimental data than the results obtained using the old hybrid solution algorithm.

4.3. Non-swirling bluff-body stabilized flame 'HM1E'

The numerical properties and performance of the present hybrid method are examined using the bluff-body stabilized flame studied experimentally by Dally et al. [4,5] and computationally using the old consistent hybrid algorithm by Muradoglu et al.

[20] and Liu et al. [14]. Here we consider the 'HM1E' flame whose details are specified in Table 2. In this table, U_c is the velocity of co-flowing air, U_j is the velocity of fuel jet and T_{in} is the temperature of fuel at jet exit plane and ξ_{st} is the stoichiometric mixture fraction. For the numerical simulations, the flame is assumed to be axisymmetric so a cylindrical coordinate system is adopted with x representing the axial direction aligned with the jet axis and r the radial direction as sketched in Fig. 4. The origin of the coordinate system is placed at the center of the fuel jet in the exit plane. The computational domain is $10D_b$ long in the axial direction and extends to $4D_b$ in the radial direction. A tensor product, orthogonal Cartesian grid is used with total of $M^2 = N_x \times N_r$ non-uniform cells. The grid is stretched both in the axial and radial directions.

The initial and boundary conditions are specified in the same way as in Muradoglu et al. [20] for all the quantities. The axial mean velocity is specified based on the assumption of a fully developed turbulent pipe flow in the jet region while it is interpolated from the experimental data in the co-flow region. The axial and radial rms fluctuating velocities (U_{RMS} and V_{RMS}) are also interpolated from the experimental data both in the jet and co-flow regions, and the mean turbulent shear stress is then calculated as

$$\widetilde{uv} = \rho_{12}\sqrt{u^2 v^2}, \tag{11}$$

where $\rho_{12} = -0.4$ and $\rho_{12} = 0.5(r/R_j)$ in the co-flow and jet regions, respectively. Velocity components are specified at the inlet such that the fluctuating velocity PDF is joint normal with zero means. Based on the assumption of equilibrium between the production and dissipation, the mean turbulent frequency is calculated as

$$\tilde{\omega} = -\frac{\widetilde{uv}}{\tilde{k}}\frac{\partial \widetilde{U}}{\partial r}. \tag{12}$$

Since the flow is dominated by the large recirculation zones and hence there is no need to resolve the boundary layer, perfect slip and no penetration boundary conditions are applied on the buff-body surface. The symmetry and far field boundary conditions are applied at the centerline and the outer boundaries, respectively. Pressure is fixed at the atmospheric pressure while the velocity is extrapolated at the exit plane.

4.3.1. Statistical stationary solution

The present hybrid method is designed to simulate statistically stationary flows. To show the statistical stationarity of the numerical solutions, time series of Favre-averaged mean axial velocity and turbulent kinetic energy are monitored at six probe locations as specified in Table 3. Fig. 5 depicts the time histories of mean axial velocity and turbulent kinetic energy at these probe points. The results are obtained using a 114×114 grid and the number of particles per cell $N_{pc} = 50$. It can be seen that a statistical stationary solution is obtained after about 8000 particle time steps, which is comparable with the old hybrid algorithm.

4.3.2. Comparison with the earlier PDF simulations and the experimental data

The results are now compared with the earlier PDF simulations performed using the old hybrid algorithm [20] and also with the experimental data [44]. Note that two sets of experimental data have been reported for the 'HM1E' flame by the same group [44]. The new data set was measured using a new experimental facility in the University of Sydney and thus expected to be more accurate. However the mixture fraction measurements were not included in the new data set. Therefore, the flow field quantities are compared with the latest experimental data while the mean and rms mixture fraction are compared with the old experimental data in which the jet and co-flow bulk velocities are set to 118 m/s and 40 m/s, respectively. An extensive study of numerical accuracy of the hybrid algorithm with respect to the grid convergence and bias error has been performed. It is found that all the results presented here are numerically accurate within 5% error tolerance as will be discussed in Sections 4.3.3 and 4.3.4.

First the mean streamlines are computed using both the old and new hybrid algorithm and plotted in the vicinity of the recirculation zone (RZ) in Fig. 6. Since the streamlines were not reported by Muradoglu et al. [20], the computations are repeated using the old loosely coupled hybrid code *HYB2D* [22]. In spite of qualitative similarity of streamline patterns in Fig. 6, the length of the recirculation zone is predicted as $\ell_r/D_b \approx 1.65$ and $\ell_r/D_b \approx 1.4$ by the present and old hybrid algorithms, respectively. Note that the present result is in better agreement with the experimental value of $\ell_r/D_b \approx 1.6$ [5]. In addition, the shape and length of RZ obtained by the new algorithm are consistent with the LES results reported by Raman and Pitsch [30] who give the length of the recirculation region as $\ell_r/D_b \approx 1.65$. For a better quantitative comparison, the radial profiles of mean axial velocity ($\widetilde{U}$), mean radial velocity ($\widetilde{V}$), the rms axial fluctuating velocity (U_{RMS}) and the rms radial fluctuating velocity (V_{RMS}) are plotted in Figs. 7–10, respectively, at the axial locations of $x/D_b = 0.06, 0.2, 0.4, 0.8, 1.0, 1.4, 1.8, 2.4$ and 3.4. These figures show that there is overall good agreement between the present results and the results obtained by the old hybrid algorithm demonstrating the accuracy of the present hybrid method. Only exception is the axial location of $x/D_b = 1.4$ where the edge of RZ is located and thus the axial velocity is significantly under predicted near the centerline by the old hybrid algorithm. In addiction, there is good agreement between the present calculations and the experimental data at the axial locations up to the end of RZ. Starting from the axial location $x/D_b = 1.8$, the results deteriorate especially near the axis of symmetry for the mean axial velocity. The rms velocities are predicted very well at most of axial locations especially before $x/D_b = 2.4$ as can bee seen in Figs. 9 and 10. Finally, the radial profiles of the mean and rms of mixture fraction are plotted in Figs. 11 and 12 at six axial locations together with the experimental data and with the earlier PDF simulations. As can be seen in these figures, the present results are overall in good agreement with the earlier PDF simulations. Compared to the experimental data, both quantities are reasonably well predicted in most of the axial locations except for the very downstream location of $x/D_b = 2.4$ where the mean mixture fraction is under predicted and between $x/D_b = 0.9$ and $x/D_b = 1.8$ where the rms mixture fraction is over predicted near the centerline.

In the summary, the present results are found to be in good agreement with the earlier PDF simulations performed using the old hybrid solution algorithm demonstrating the accuracy of the new hybrid method. Thus the differences between computational and experimental results are mainly attributed to the deficiency of the sub-models. However, considering the fact that the simplest sub-models are used in the present calculations, the performance of the PDF model is remarkable and is expected to improve significantly when more advanced models are employed.

4.3.3. Spatial error

Extensive simulations are performed to demonstrate grid convergence of the present hybrid method by successively refining the computational grid from 64×64 up to 216×216. The spatial

Table 4
The non-swirling bluff-body HM1E flame. Percentage spatial discretization error for mean and fluctuating quantities obtained with various grid resolutions.

Quantities	$\widetilde{U}$	$\widetilde{V}$	U_{RMS}	V_{RMS}	Ω	$\widetilde{\xi}$	ξ_{RMS}
64×64	16.5	21.2	23.2	31.0	15.5	12.2	21.1
96×96	12.8	16.3	15.0	20.2	10.5	8.5	14.0
144×144	7.8	9.1	4.7	8.5	6.6	4.0	6.4
216×216	4.7	4.9	2.6	2.9	2.0	2.8	3.1

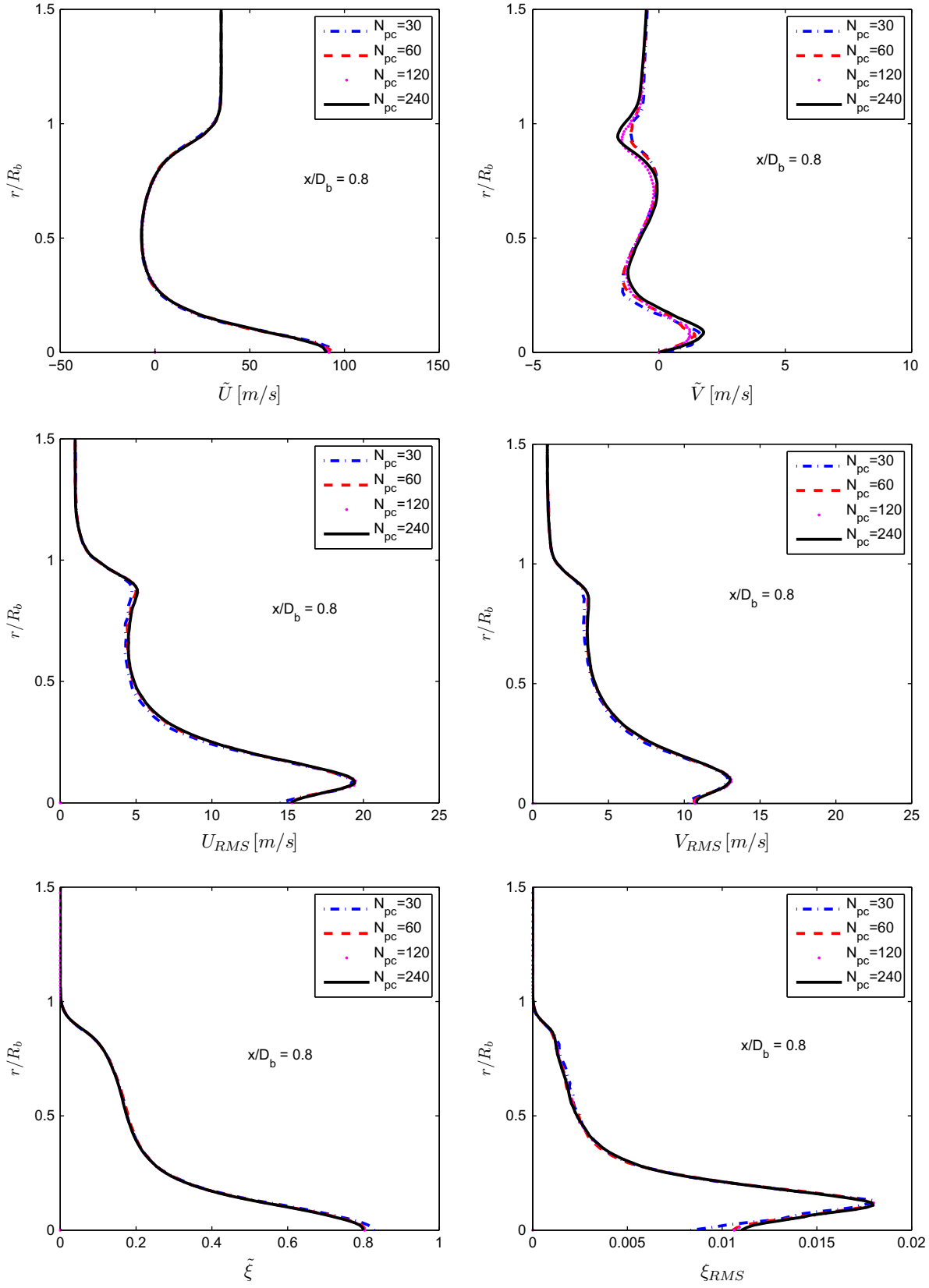

Fig. 15. Bias error for the non-swirling bluff-body HM1E flame: radial profiles of mean and rms fluctuating axial and radial velocities, mean and rms mixture fraction at axial location $x/D_b = 0.8$.

error results from the spatial discretization in the finite-volume method and also from the kernel estimation and interpolation schemes used in the particle algorithm. All the simulations are performed with the number of particles per cell $N_{pc} = 50$ and the time-averaging factor $N_{TA} = 500$. The time-averaged profiles of mean axial and radial velocity, rms axial and radial velocities,

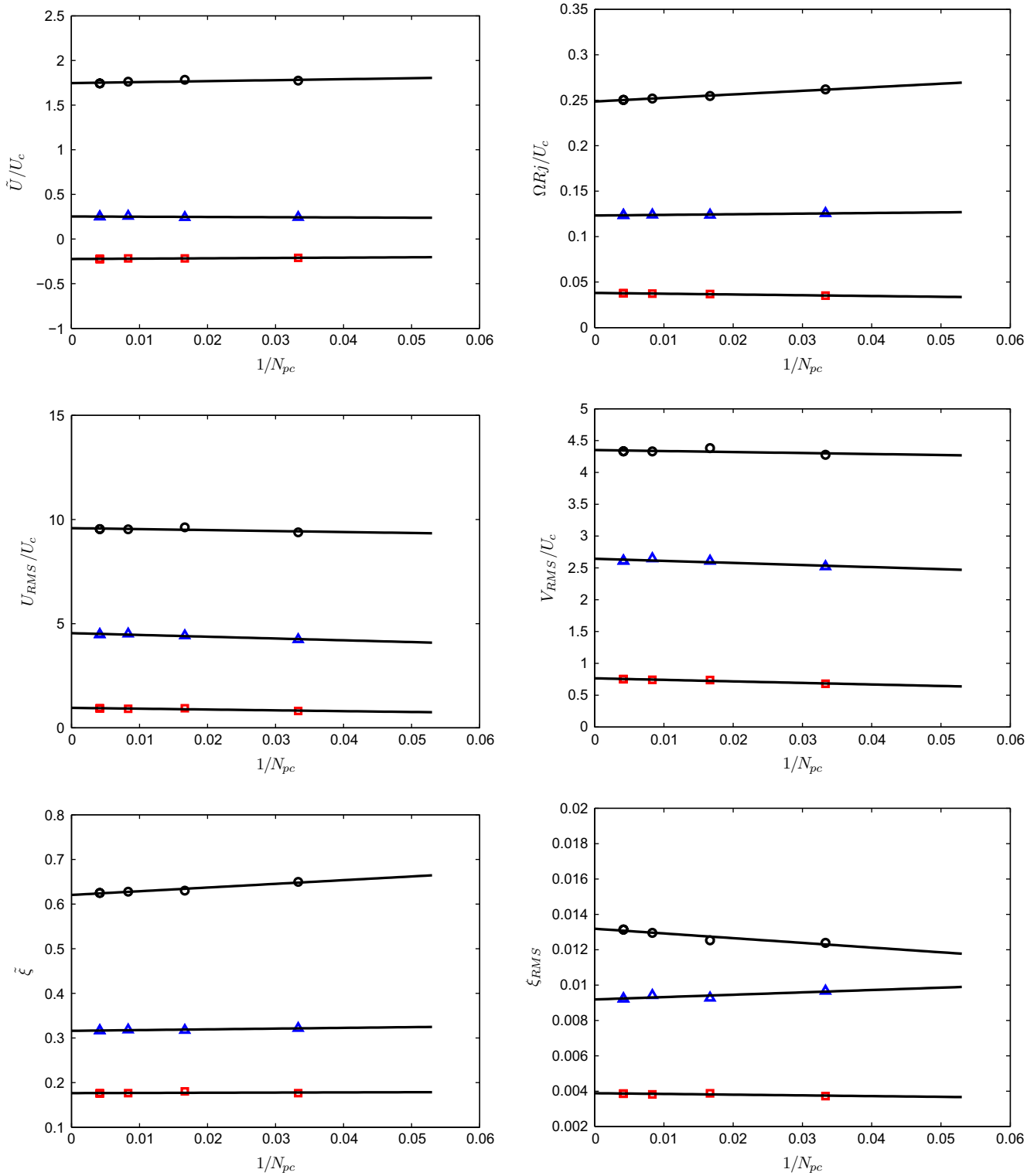

Fig. 16. Bias error for the non-swirling bluff-body HM1E flame: mean and fluctuating quantities against $1/N_{pc}$ at selected points. Circles indicate the location at $(x/D_b = 1.0, r/R_j = 1)$, triangles at $(x/D_b = 1.0, r/R_b = 0.5)$, squares at $(x/D_b = 1.0, r/R_b = 1.0)$, and solid lines show the linear least squares fits to the computational results.

and mean and rms mixture fraction are plotted in Fig. 13 at the axial location $x/D_b = 0.4$ to show overall dependence of the calculated results on the grid refinement. As can be seen in these figures, the difference among the profiles is decreasing with grid refinement, indicating that grid convergence is achieved. To verify the second-order spatial accuracy of the method, the mean quantities, $\widetilde{U}, \Omega, U_{RMS}, V_{RMS}, \tilde{\xi}$ and ξ_{RMS} are also plotted against the inverse of total number of grid cells M^{-2} at the locations $(x/D_b, r/R_j) = (1,1), (x/D_b, r/R_b) = (1, 0.5)$ and $(x/D_b, r/R_b) = (1,1)$ in Fig. 14 where the symbols represent the numerical data and the solid lines are the linear least-squares fits to the data. As can be seen in this figure, the approximate linear relationship between the mean quantities and M^{-2} confirms the expected second-order spatial accuracy of the method. Assuming a second order accuracy

Table 5
The non-swirling bluff-body HM1E flame. Percentage bias error for mean and fluctuating quantities obtained using various number of particles per cell.

Quantities	$\widetilde{U}$	$\widetilde{V}$	U_{RMS}	V_{RMS}	Ω	$\widetilde{\xi}$	ξ_{RMS}
$N_{pc} = 30$	8.7	9.2	6.0	5.4	7.5	2.7	7.3
$N_{pc} = 60$	2.5	3.3	2.9	1.3	3.9	1.8	3.4
$N_{pc} = 120$	2.4	2.7	1.9	1.1	3.3	0.6	2.9
$N_{pc} = 240$	1.2	1.5	1.6	1.0	1.0	0.4	0.6

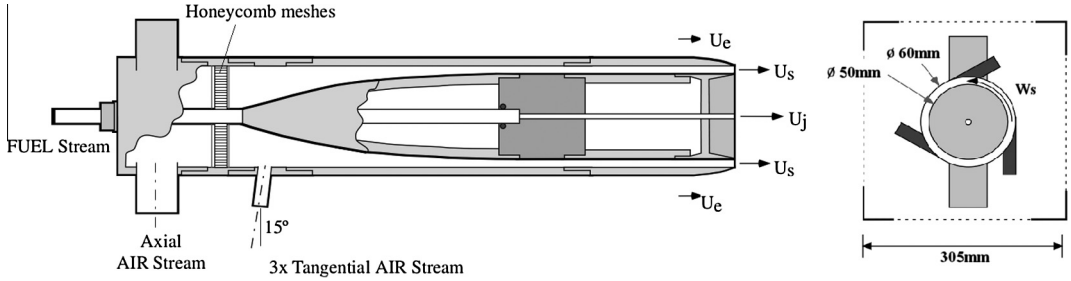

Fig. 17. A schematic drawing of the Sydney swirling bluff-body burner (adopted from Al-Abdeli and Masri [1]).

Table 6
Flow parameters for the swirling bluff-body flame 'SM1'.

Case	Fuel	U_c (m/s)	U_j (m/s)	U_s (m/s)	W_s (m/s)	S_g
SM1	CH4	20	32.7	38.2	19.1	0.5

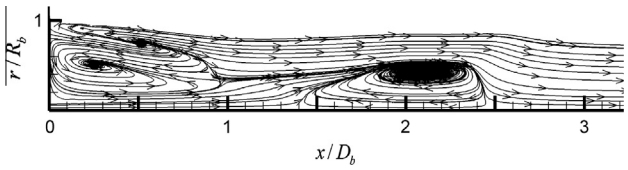

Fig. 19. The swirling bluff-body flame 'SM1'. The streamlines of the mean velocity computed for the swirling bluff-body flame in the vicinity of the recirculation zones.

and using the Richardson extrapolation, the spatial error free values are obtained from Fig. 14 as $M \to \infty$ and then the relative error is computed as

$$\epsilon = \frac{|Q_M - Q_\infty|}{|Q_\infty|}, \tag{13}$$

where Q_M is the numerical result obtained using a grid with M^2 grid cells and Q_∞ is predicted using Richardson extrapolation as $M \to \infty$. Table 4 summarizes the average percentage spatial error at the six probe points. As can be seen in this table, a grid containing 216×216 cells is sufficient for the spatial error to be less than 5% in all the mean quantities at these locations.

4.3.4. Bias error

Bias error is a deterministic numerical error caused by the fluctuations in the particle mean fields used in the equations solved by the particle method. The bias error is expected to scale as N_{pc}^{-1} where N_{pc} is the number of particles per cell [40]. Although the bias error was a major problem in the stand alone particle method [40], it has been shown that it is virtually eliminated in the consistent hybrid approach [23,12,22]. Extensive simulations are performed here to quantify the bias error in the present hybrid method using a 216×216 grid. The time-averaged profiles of the mean axial and radial velocities, the rms fluctuating axial and radial velocities, and the mean and rms mixture fraction at the axial location $x/D_b = 0.8$ are plotted in Fig. 15 for $N_{pc} = 30, 60, 120$ and 240. Time averaging parameter is set to $N_{TA} = 500$ to reduce the statistical fluctuations. As can be seen in this figure, the profiles are close to each other indicating that the bias error is small. Fig. 16 shows the time-averaged and normalized mean and fluctuating values of flow quantities against N_{pc}^{-1} at the locations $(x/D_b, r/R_j) = (1, 1), (x/D_b, r/R_b) = (1, 0.5)$ and $(x/D_b, r/R_b) = (1, 1)$. The approximate linear relationship between the mean quantities and N_{pc}^{-1} confirms the expected

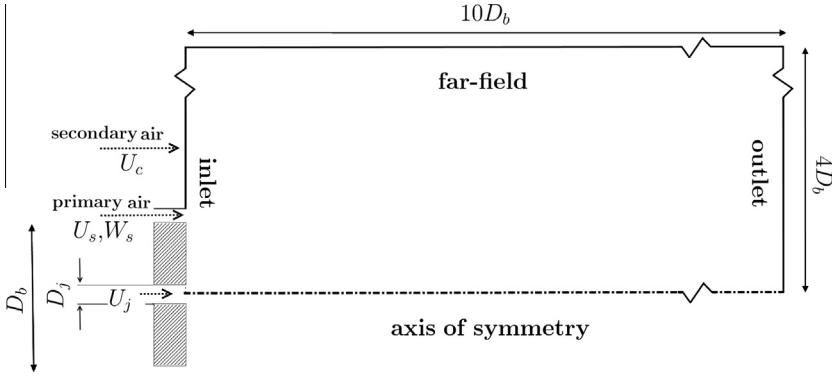

Fig. 18. Computational domain for the swirling bluff-body flame 'SM1'.

scaling of the bias error. The slopes of the lines indicate the sensitivity of the solutions to the bias error. The average bias error at the six probe points are summarized in Table 5. The relative bias error is calculated as

$$\epsilon = \frac{|Q_{N_{pc}} - Q_{N_{pc}\to\infty}|}{|Q_{N_{pc}\to\infty}|}, \tag{14}$$

where $Q_{N_{pc}}$ is the numerical result obtained using N_{pc} particles per cell and $Q_{N_{pc}\to\infty}$ is predicted using the Richardson extrapolation as $N_{pc} \to \infty$. It can be seen that the bias error for a given value of N_{pc} in the present hybrid method is much smaller than the stand-alone particle/mesh method [40], and comparable to the bias error in the old hybrid algorithm. It is also seen in these figures that $N_{pc} = 50$ is sufficient to virtually eliminate the bias error compared to the spatial error on a typical grid used.

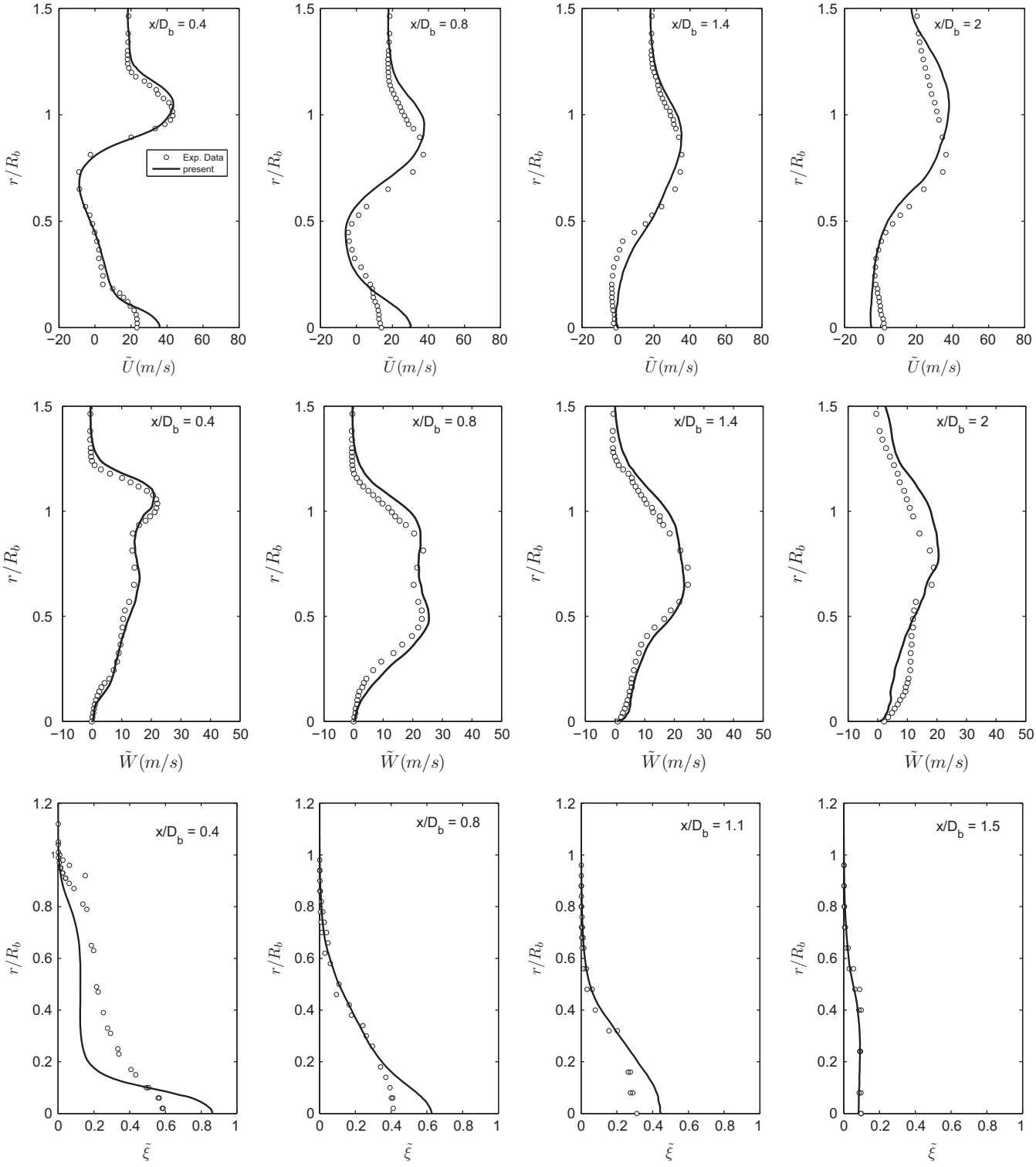

Fig. 20. The swirling bluff-body flame 'SM1'. The profiles of mean axial and tangential velocities at the axial locations of $x/D_b = 0.4, 0.8, 1.4$ and 2, and the mean mixture fraction at the axial locations of $x/D_b = 0.4, 0.8, 1.1$ and 1.5. The solid lines indicate the computational results and the symbols are the experimental data [44].

4.4. Swirling bluff-body flame 'SM1'

The hybrid method is finally applied to simulate the more difficult test case of swirling bluff-body flame studied experimentally by the University of Sydney group [1,13,15]. It is known that the swirling bluff-body flame exhibit significant unsteadiness due to precessing of the recirculation zone in axial direction [1,13,15]. As mentioned before, the present hybrid method is designed to simulate only statistically stationary flows, so the case labeled as 'SM1' is chosen as a test case here since it exhibits the least precession. A schematic configuration of Sydney swirl burner is shown in Fig. 17. It has a 50 mm diameter bluff-body ($D_b = 50$ mm) with a 3.6 mm diameter central fuel jet. Swirling air is provided through a 60 mm diameter annulus surrounding the bluff-body. The burner is placed inside a wind tunnel with a square cross section. An extensive experimental study has been performed for this flame [1,13,15] and the experimental data are freely available from the Internet [44,42]. Different swirling bluff-body flames are distinguished by five independent parameters: The bulk axial velocity of the central jet (U_j), the bulk axial and tangential velocities of the swirling air annulus (U_s and W_s), the bulk axial velocity of the co-flow of the wind tunnel (U_c) and also with the type of fuel. Here we consider the case 'SM1' for which the flow parameters are summarized in Table 6. Here S_g is geometric swirl number defined as $S_g = W_s/U_s$.

As for the non-swirling case, the flow is assumed to be statistically axisymmetric so a cylindrical coordinate system is adopted. The origin of the coordinate system is located on the centerline of the jet exit plane ($x = 0, r = 0$). The computational domain is rectangular that extends 0.5 m ($10D_b$) in the axial direction downstream of bluff-body and 0.2 m ($4D_b$) in the radial direction as sketched in Fig. 18. The boundary conditions are specified as follows: The mean axial velocity is specified assuming a fully-developed turbulent pipe flow and the experimental data are used in the primary swirling air stream for axial and tangential velocities as well as for the axial velocity in the co-flow region. Full slip boundary conditions are applied on the surface of the bluff-body wall.

The new hybrid algorithm is applied to simulate the flame 'SM1'. The main purpose here is to demonstrate the robustness of the present hybrid method for this challenging test case. Therefore a few results are presented here and the complete description of the results with a flamelet and a detailed chemistry models will be reported separately. The same models for fluctuating velocity, turbulent frequency, chemistry and mixing are employed for this flame as used for the non-swirling case. Although not shown here due to space consideration, the solution reaches a statistical stationary state after about 7000 particle time steps. Fig. 19 depicts the computed mean streamlines in the recirculation region behind the bluff-body. As can be seen in this figure, two recirculation regions are well captured by the present calculations. The first recirculation zone (RZ) is created by the circular bluff body immediately behind the bluff-body base similar to the non-swirling case. The second recirculation is induced by the swirl around the centerline and is called a vortex breakdown bubble (VBB). The overall flow structure is in good agreement with the experimental observation [1]. The upstream RZ has two vortices similar to the non-swirling case. The center of the first vortex is located at $x/D_b \approx 0.25$ while the second one is located at $x/D_b \approx 0.5$ and extends up to $x/D_b \approx 1.0$. The VBB is located between $x/D_b \approx 1.4$ and $x/D_b \approx 2.4$. Experimental results indicate that the the first RZ extends up to $x/D_b \approx 1.0$ while the second RZ starts at about $x/D_b \approx 1.3$ and extends up to about $x/D_b \approx 2.2$ [13], showing that the present results are in good agreement with the experimental observations. Fig. 20 shows the computed and experimental radial profiles of mean axial and tangential velocities as well as the mean mixture fraction. Considering the fact that the simplest velocity, chemistry and mixing models are employed here, the computational results are remarkably in good agreement with the experimental data. It is also emphasized here that the hybrid algorithm is found to be very robust for this test case against grid refinement.

5. Conclusions

A new robust consistent hybrid FV/particle method has been developed for solving PDF model equations of turbulent reacting flows as a first step toward developing a general purpose RANS/PDF and LES/PDF solver within the framework of the open source software package, OpenFOAM. The new hybrid method is designed to eliminate the deficiencies of the original hybrid algorithm such as excessive numerical dissipation and lack of robustness with respect to grid refinement while retaining all the advantages of the consistent hybrid approach.

In the new hybrid method, a pressure-based PISO-FV solver is combined with the particle-based Monte Carlo algorithm. The mean density field is extracted from the particles and passed to the FV solver. This is in contrast with the old hybrid approach in which the mean energy conservation equation is solved by the FV method and mean density field is subsequently computed from the mean equation of state. Thus the redundant FV density field is removed in the present approach. This is of significance since it makes the new hybrid algorithm more consistent at the numerical solution level and eliminates the need for the energy correction algorithm. In spite of noisy mean density field, the FV algorithm is found to be very robust. The velocity and position correction algorithms developed by Muradoglu et al. [22] are adopted to make the new hybrid method fully consistent at the numerical solution level. The local time stepping method developed by Muradoglu and Pope [21] has been also incorporated into the present hybrid algorithm and found to accelerate convergence to a statistically stationary solution significantly especially when a highly stretched grid is used.

The new hybrid algorithm is first applied to simulate the non-swirling cold bluff-body flow. In contrast with the original hybrid method, the new hybrid method is found to be very robust with respect to grid refinement, i.e., it does not result in any unphysical vortex shedding even when a highly fine grid is used. It is thus concluded that the unphysical vortex shedding observed by Jenny et al. [12] was not due to the deficiency of the models employed but rather due to the excessive numerical dissipation in the density-based FV solver used in the old loosely-coupled hybrid method. The method is then applied to simulate the non-swirling reacting bluff-body flame 'HM1E'. It is found that the new hybrid method predicts the flow field in the recirculation region better than the old hybrid algorithm. Extensive simulations are then performed for this flame to assess the numerical properties of the present hybrid algorithm. It is demonstrated that the method is convergent in terms of reaching a statistically stationary state and also in terms of grid refinement and number of particles per cell. It is found that both the bias and spatial errors converge at expected rates and the bias error is much smaller than the spatial error on a typical grid employed in PDF simulations, i.e., the bias error is virtually eliminated. Finally the robustness of the new algorithm is demonstrated by simulating more complicated flow of the Sydney swirling bluff-body flame 'SM1'. The new algorithm is found to be very robust for this difficult test case and the results are in good agreement with the available experimental data.

The future work includes the application of the present hybrid method to simulate the non-swirling and swirling bluff-body flames using a detailed chemistry model and development of a

LES/PDF method within the OpenFOAM framework as laid out in the present study.

Acknowledgement

The authors are grateful to the Scientific and Technical Research Council of Turkey (TUBITAK) for the support of this research through Grant 111M067 and Turkish Academy of Sciences (TUBA).

References

[1] Al-Abdeli YM, Masri AR. Stability characteristics and flow fields of turbulent non-premixed swirling flames. Combust Theor Model 2003;7:731–66.
[2] Bilger RW, Starner SH, Kee RJ. On reduced mechanisms for methane–air combustion in non-premixed flames. Combust Flame 1990;80:135–49.
[3] Cao R, Wang H, Pope SB. The effect of mixing models in PDF calculations of piloted jet flames. Proc Combust Inst 2007;31:1543–50.
[4] Dally BB, Masri AR, Barlow RS, Fiechtner GJ. Instantaneous and mean compositional structure of bluff-body stabilized non-premixed flames. Combust Flame 1998;114:119–48.
[5] Dally BB, Fletcher DF, Masri AR. Flow and mixing fields of turbulent bluff-body jets and flames. Combust Theor Model 1998;2:193–219.
[6] Dopazo C, O'Brien EE. An approach to the autoignition of a turbulent mixture. Acta Astronaut 1974;1:1239–66.
[7] Darmofal DL, Schmid PJ. The importance of eigenvectors for local preconditioners of the Euler equations. J Comput Phys 1996;127:346–62.
[8] Haworth DC, Pope SB. A generalized Langevin model for turbulent flows. Phys Fluids 1986;29:387–405.
[9] Hockney RW, Eastwood JW. Computer simulations using particles. NewYork: Adam Hilger; 1988.
[10] Issa RI. Solution of the implicitly discretized fluid flow equation by operator splitting. J Comp Phys 1986;62:40–65.
[11] Jenny P, Pope SB, Muradoglu M, Caughey DA. A hybrid algorithm for the joint PDF equation for turbulent reactive flows. J Comp Phys 2001;166:218–52.
[12] Jenny P, Muradoglu M, Liu K, Pope SB, Caughey DA. PDF simulations of a bluff-body stabilized flow. J Comp Phys 2001;169:1–23.
[13] Kalt PAM, Al-Abdeli YM, Masri AR, Barlow RS. Swirling turbulent non-premixed flames of methane: flow field and compositional structure. Proc Combust Inst 2002;29:1913–7.
[14] Liu K, Caughey DA, Pope SB. Calculations of bluff-body stabilized flames using a joint probability density function model with detailed chemistry. Combust Flame 2005;141:89–117.
[15] Masri AR, Kalt PAM, Barlow RS. The compositional structure of swirl-stabilized turbulent non-premixed flames. Combust Flame 2004;137:1–37.
[16] Masri AR, Dally BB, Barlow RS, Carter CD. The structure of the recirculation zone of a bluff-body combustor. Proc Combust Inst 1994;25:1301–7.
[17] Meyer DW, Jenny P. Micromixing models for turbulent flows. J Comp Phys 2009;228:1275–93.
[18] Meyer DW, Jenny P. Accurate and computationally efficient mixing models for the simulation of turbulent mixing with PDF methods. J Comp Phys 2013;247:192–207.
[19] Muradoglu M, Caughey DA. Implicit multigrid solution of the multi-dimensional preconditioned Euler equations. AIAA paper 98-0114; 1998.
[20] Muradoglu M, Liu K, Pope SB. PDF modeling of a bluff-body stabilized turbulent flame. Combust Flame 2003;132:115–37.
[21] Muradoglu M, Pope SB. Local time-stepping algorithm for solving probability density function turbulence model equations. AIAA J 2002;40:1755–63.
[22] Muradoglu M, Pope SB, Caughey DA. The hybrid method for the PDF equations of turbulent reactive flows: consistency conditions and correction algorithms. J Comp Phys 2001;172:841–78.
[23] Muradoglu M, Jenny P, Pope SB, Caughey DA. Hybrid finite-volume/particle method for the PDF equations of turbulent reactive flows. J Comp Phys 1999;154:342–71.
[24] Pope SB. A model for turbulent mixing based on shadow-position conditioning. Phys Fluids 2013;25:110803.
[25] Pope SB, Hiremath V, Lantz SR, Ren Z, Lu L. A Fortran 90 library to accelerate the implementation of combustion chemistry 2012. <http://tcg.mae.cornell.edu/ISATCK7>.
[26] Pope SB. Lagrangian PDF methods for turbulent flows. Ann Rev Fluid Mech 1994;26:23–63.
[27] Pope SB. pdf2dv: a Fortran code to solve the modeled joint PDF equations for two-dimensional recirculating zones 1994. Unpublished, Cornell University.
[28] Pope SB. On the relationship between stochastic Lagrangian models of turbulence and second-moment closures. Phys Fluids 1994;6:973–85.
[29] Pope SB. PDF methods for turbulent reactive flows. Prog Energy Combust Sci 1985;11:119–92.
[30] Raman V, Pitsch H. Large-eddy simulation of a bluff-body-stabilized non-premixed flame using a recursive filter-refinement procedure. Combust Flame 2005;142:329–47.
[31] Rowinski DH, Pope SB. An investigation of mixing in a three-stream turbulent jet. Phys Fluids 2013;25:105105.
[32] Sawford B. Lagrangian modeling of scalar statistics in a double scalar mixing layer. Phys Fluids 2006;18:085108.
[33] Subramaniam, Pope SB. A mixing model for turbulent reactive flows based on Euclidean minimum spanning trees. Combust Flame 1998;115:487–514.
[34] Sweeney MS, Hochgreb S, Dunn MJ, Barlow RS. The structure of turbulent stratified and premixed methane/air flames I: non-swirling flows, combustion flame. Combust Flame 2012;159:2896–911.
[35] Tang Q, Xu J, Pope SB. Probability density function calculations of local extinction and no production in piloted-jet turbulent methane/air flames. Proc Combust Inst 2000;28:133–9.
[36] Turkel E. Preconditioned methods for solving the incompressible and low speed compressible equations. J Comput Phys 1987;72(2):277–98.
[37] Turkel E, Radespiel R, Kroll N. Assessment of preconditioning methods for multidimensional aerodynamics. Comput Fluids 1997;26:613–34.
[38] Van Slooten PR, Jayesh, Pope SB. Advances in PDF modeling for inhomogeneous turbulent flows. Phys Fluids 1998;10:246–65.
[39] Xu J, Pope SB. PDF calculations of turbulent non-premixed flames with local extinction. Combust Flame 2000;123:281–307.
[40] Xu J, Pope SB. Assessment of numerical accuracy of PDF/Monte Carlo methods for turbulent reacting flows. J Comp Phys 1999;152:192–230.
[41] GRI Mechanism 2.1. <http://www.gri.org>.
[42] International workshop on measurement and computation of turbulent non-premixed flames (TNF). <http://www.sandia.gov/TNF>.
[43] OpenFOAM. The open source CFD toolbox, OpenFOAM. <http://www.openfoam.com/>; 2013.
[44] University of Sydney. Clean combust. Research group. <http://sydney.edu.au/engineering/aeromech/thermofluids>.